Buffer Catalysis for the Hydrolysis and the *Carbonyl*-^{18}O Exchange of *N*-*p*-Nitrobenzoylpyrrole

by

Laurence J. Beach
B. Sc. University of British Columbia, 1991

THESIS SUBMITTED IN PARTIAL FULFILLMENT
OF THE REQUIREMENTS FOR THE DEGREE OF
MASTER OF SCIENCE
in the Department of
Chemistry

© Laurence J. Beach 1995
SIMON FRASER UNIVERSITY
November 1995

All rights reserved. This work may not be reproduced in whole or in part, by photocopy or other means, without permission of the author.

Approval

Name: Laurence J. Beach

Degree: Master of Science (Chemistry)

Title of Thesis: Buffer Catalysis for the Hydrolysis and the *Carbonyl*-^{18}O Exchange of *N*-*p*-Nitrobenzoylpyrrole

Examining Committee:

Chairperson: Dr. S. Holdcroft, Associate Professor

Dr. A. J. Bennet
Assistant Professor
Senior Supervisor

Dr. R. H. Hill
Associate Professor

Dr. B. M. Pinto
Professor

Dr. K. N. Slessor
Professor
Internal Examiner

DATE APPROVED: November 23, 1995

PARTIAL COPYRIGHT LICENSE

I hereby grant to Simon Fraser University the right to lend my thesis, project or extended essay (the title of which is shown below) to users of the Simon Fraser University Library, and to make partial or single copies only for such users or in response to a request from the library of any other university, or other educational institution, on its own behalf or for one of its users. I further agree that permission for multiple copying of this work for scholarly purposes may be granted by me or the Dean of Graduate Studies. It is understood that copying or publication of this work for financial gain shall not be allowed without my written permission.

Title of Thesis/Project/Extended Essay:

Buffer Catalysis for the Hydrolysis and the *Carbonyl*-^{18}O Exchange of *N*-*p*-Nitrobenzoylpyrrole

Author:

(signature)

Laurence Beach

(name)

November 23, 1995

(date)

Abstract

The observed rate constants for the hydrolysis of *N*-*p*-nitrobenzoylpyrrole (**1**) (T = 25 °C, concentration ionic strength, μ = 1.00 M (KCl)) in the presence of two buffers (1,4-diazabicyclo[2.2.2]octane (DABCO) and trimethylamine (TMA)) were calculated from UV absorbance versus time data. The second-order rate constant for hydroxide ion-promoted hydrolysis of **1** with no added buffer was calculated (37 ± 1 $M^{-1}s^{-1}$). The partitioning of the anionic tetrahedral intermediate (To^-) was calculated in the absence of a buffer by the ratio of the rates of *carbonyl*-^{18}O exchange and hydrolysis ($k_{ex}/k_{hyd} = 0.05 \pm 0.02$). The buffer-promoted To^- partitioning, k_{BH}/k_{BP} (reversal to amide/formation of products), from the proposed scheme for the hydrolysis of **1** in the presence of added DABCO was calculated from the *carbonyl*-^{18}O exchange data and corresponding DABCO concentrations ($k_{BH}/k_{BP} = 1.0 \pm 0.06$). The observed solvent kinetic isotope effect (SKIE) for the buffer-promoted hydrolysis of **1** was $k_{H2O}/k_{D2O} > 1$. The value is consistent with general base-promoted To^- formation. The crystal structure of **1** was analysed and compared with that of *N*-toluoylpyrrole (**2**). No structural reasons could be provided for the occurrence of buffer catalysis in **1** and not in **2**.

Acknowledgment

I would like to thank the following people:

Dr. Andrew Bennet, my senior supervisor, for all of his guidance and help;

Dr. Mario Pinto and Dr. Ross Hill, of my supervisory committee, for their ideas and suggestions for this work;

Mr. Greg Owen, for his help and patience with the mass spectrometric data;

Dr. Raymond Batchelor, for his guidance and analysis of the x-ray crystallographic data;

The Department of Chemistry, for its support throughout the course of my work;

Dr. Harry Davis, Ms. Shannon Harris, Dr. Mohamed Abdou for their help;

And my loving wife, Eliza, for her loving support and patience during this work.

Table of Contents

List of Tables

List of Figures

List of Abbreviations

α	position of transition state on reaction cooordinate
λ	wavelength
μ	concentration ionic strength
ν	reaction rate
π	molecular orbital of pi symmetry
υ_L	vibrational frequency involving H or D
Φ	fractionation factor
χ^2_P	chi square statistic
χ_C	pyramidalisation at carbon
χ_N	pyramidalisation at nitrogen
A	amide
Å	angstrom
Acyl	acyl group
asp	aspartic acid
B	basic buffer species
BH^+	acidic buffer species
CAD	carboxylic acid derivative
DABCO	1,4-diazabicyclo[2.2.2]octane
DME	1,2-dimethoxyethane
E	enzyme
$E_{\upsilon i}$	vibrational energy level
f	force constant
gly	glycine
hr	hour
his	histidine
HOMO	highest occupied molecular orbital
HPLC	high-performance liquid chromatography
k	rate constant
L	H or D
Lg^-	leaving group (normally amido or alkoxide)
LUMO	lowest unoccupied molecular orbital
M	moles/litre
NMR	nuclear magnetic resonance
n_X	nonbonding electron pair on species X
O^*	Oxygen-18
pH	$-\log[H^+]$
Phe	phenylalanine
pK_a	$-\log(K_a)$, K_a = acid dissociation constant
pOL	$-\log[OL^-]$

R	organic substituent
s	second
SKIE	solvent kinetic isotope effect
T	temperature (°C)
THF	tetrahydrofuran
TI	generic tetrahedral intermediate
TMA	trimethylamine
To^-	anionic tetrahedral intermediate
TS	transition state
[X]	concentration of species X

Chapter 1

Introduction

1.1 Amides in Biological Systems

The amide C–N bond (Figure 1) is important in biological systems because it is the bond that links amino acids (Figure 2) together to make a protein or polypeptide of the type in Figure 3.[1] Although the reaction half-lives for the hydrolysis of an amide can vary considerably, the amide is among the most hydrolytically stable carboxylic acid derivatives in aqueous media.[2] At pH 7, and in the absence of hydrolytic enzymes (proteases), the C–N bond of an amide is resistant to cleavage by hydrolysis.[3] However, in the presence of an enzyme, the same amide can be hydrolysed readily. What, then, does the protease do to enhance the hydrolytic rate? Part of the answer may be found in the study of the aqueous base-promoted hydrolysis of amides in the presence or absence of an added buffer.

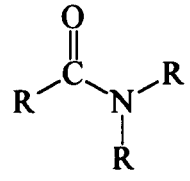

Figure 1. Generic amide. R may be a combination of alkyl or aryl groups.

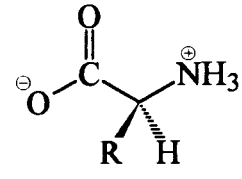

Figure 2. Isolated generic L-amino acid. Exists as zwitterion (as shown) in neutral aqueous media.

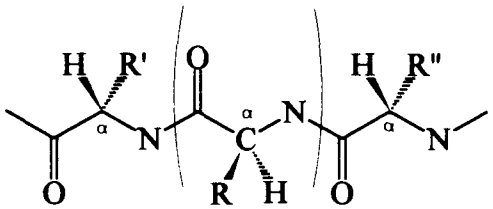

Figure 3. Three generic amino acid residues of a polypeptide or protein linked together with C–N amide bonds.

The cleavage of a protein or polypeptide into its individual amino acids is an important step in the synthesis of proteins in biological systems.[1] In order to cleave a protein into amino acids, a protease must overcome the hydrolytic kinetic barriers encountered during the hydrolysis of an amide. A protease must interact with the amide to reduce these barriers and enhance the hydrolysis rate. Interactions that stabilise the ground state of the amide group, and stabilise any of the intermediates formed during the enzyme-catalysed hydrolysis will cause a rate enhancement. By observing amide hydrolysis in the absence of an enzyme, the origins of the hydrolytic barriers in amides may be determined.

1.2 Carboxylic Acid Derivatives

1.2.1 Hydroxide Ion-Promoted Hydrolysis of Carboxylic Acid Derivatives

Amides belong to a large class of organic compounds called carboxylic acid derivatives (CAD), all of which may be hydrolysed in aqueous media. The hydroxide ion-promoted hydrolysis of a CAD is normally an addition-elimination scheme[2] (Figure 4), and involves a CAD and a hydroxide ion. In the addition step represented by the rate constant,

k_A, the hydroxide ion attacks the carbonyl carbon of the CAD to form the anionic tetrahedral intermediate (To^-) in Figure 4. The total rate for To^- formation is $k_A[OH^-][CAD]$, where k_A is a second-order rate constant for hydroxide ion-promoted To^- formation, $[OH^-]$ is the concentration of the hydroxide ion, and [CAD] is the concentration of the CAD. For amides, nucleophilic attack other than by hydroxide ions in aqueous basic media is not generally observed. Alternative nucleophiles to hydroxide ions are usually bulkier, so the formation of a To^- with a nucleophile other than a hydroxide ion is sterically hindered.[4] The term 'hydroxide ion catalysis' is often used. In a catalytic scheme, the catalyst must not be consumed by the reaction.[5] However, hydroxide ions are consumed during the hydroxide ion-promoted hydrolysis of an amide in Figure 4, so hydroxide ions do not formally catalyse the reaction. Instead, the term 'promoted' will be used throughout to refer to processes that cannot be shown to be truly catalytic.

The principle of microscopic reversibility states that, for any reaction, the product may revert to the reactants via the same mechanistic pathway and transition state through which the product was formed.[6] Thus, according to the principle of microscopic reversibility, the To^- may revert to the CAD and hydroxide ion by eliminating the hydroxide ion through the same transition state that lead to To^- formation. This reversibility is often observed during the hydrolysis of amides[7,8] so the total rate of To^- reversion to the CAD and hydroxide ion must be included. The total rate is $k_{-A}[To^-]$, where k_{-A} is the first-order rate constant for To^- reversion and $[To^-]$ is the concentration of To^-.

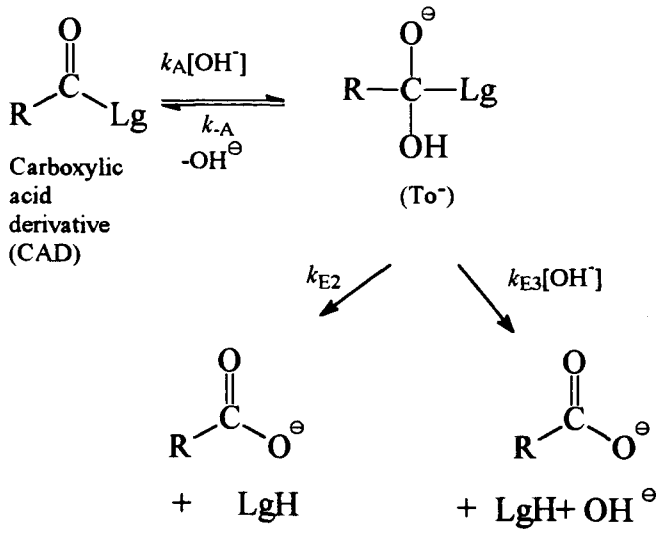

Figure 4. Scheme for the hydroxide ion-promoted hydrolysis of a carboxylic acid derivative.

In addition to To^- reversion to the CAD (k_{-A}), the To^- may also eliminate the leaving group (Lg) as a Lg^- or LgH. The elimination of either a Lg^- or LgH involves either the unimolecular To^- breakdown or the hydroxide ion-catalysed breakdown of To^- to form carboxylate and LgH, ultimately. The final products, whether the To^- eliminates a Lg^- or LgH, are normally LgH and carboxylate.[8] The total rate for To^- breakdown is $k_{E2}[To^-]$ for the unimolecular breakdown, or $k_{E3}[To^-][OH^-]$ for the hydroxide ion-catalysed breakdown.

Although the principle of microscopic reversibility requires that To^- breakdown to a product be reversible, this is not experimentally observed in aqueous basic media.[6] The product, carboxylate, is thermodynamically more stable than the starting carboxylic acid derivative. Because To^- formation from the products has not been observed during hydroxide ion-promoted hydrolysis of the CAD,[6] this process is ignored for the scheme in Figure 4 for the hydroxide ion-promoted hydrolysis of the CAD.

1.2.2 Electronic Characteristics of Amide Bonds and Related Functional Groups

Rate constants for aqueous base-promoted To^- formation, rotational barriers about the C–N bond of amides, and other experimental observations[9] have been rationalised by electronic descriptions of CAD.[10] In particular, the magnitudes of the rate constants for To^- formation during aqueous base-promoted hydrolysis of the various amides have been rationalised by the use of resonance theory, and more recently, structural arguments.[11]

Resonance theory has been customarily invoked to rationalise many of these experimental observations.[10,12,13] Conventionally, the interactions between the carbonyl C=O and Lg in amides and esters are summarised by the three resonance structures given in Figures 5 and 6, respectively. The resonance structures illustrate the delocalisation of the lone pair on L across the C–Lg bond, resulting in a partial double C–Lg bond.

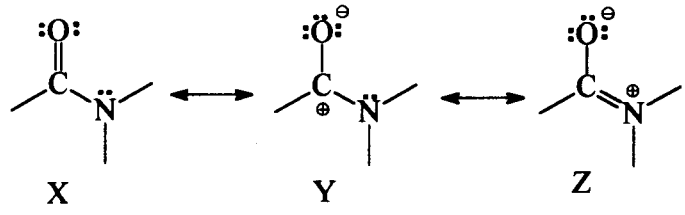

Figure 5. Resonance structures for an amide.

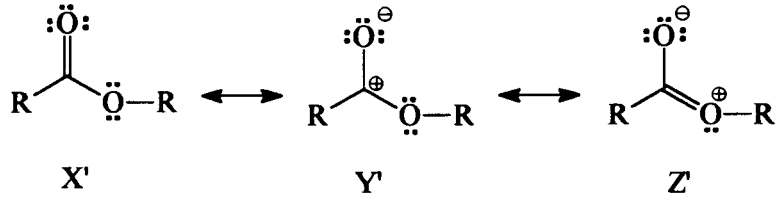

Figure 6. Resonance structures for an ester.

The observed structures for amide and ester functionalities contain some contribution from the resonance structures Z and Z' for the amide and ester, respectively, which represents the electron delocalisation within the CAD. Generally, the contribution

of the ester resonance structure Z' is less important than the contribution of the amide resonance structure Z to the overall structures of the ester and amide functionalities, respectively. Consequently, resonance theory predicts more single carbonyl C–O bond order and a less electrophilic carbonyl carbon for an amide than an ester. The effects on the bonding at the carbonyl C–O bond that are predicted by resonance theory are supported by evidence from the IR stretching frequencies of the carbonyl C=O. The ester carbonyl C=O stretching frequency is about 1730 cm^{-1} while that of the amide is about 1650 cm^{-1}. The lower value for the amide carbonyl C–O stretching frequency corresponds with the reduced bond order[14] in the amide C–O bond predicted from resonance theory. The stretching frequency for a single carbonyl C–O bond is about 1000–1260 cm^{-1}. If the IR stretching frequencies may be correlated with the bond order, the carbonyl C–O bond order in the amide is closer to a single carbonyl C–O bond than that of the ester carbonyl C–O bond.

Bender, Ginger and Unik[15] calculated the second-order rate constants, k_1, for To^- formation during the hydrolyses of ethyl benzoate and benzamide (Figure 7) in aqueous basic media. The rate of To^- formation from the ester is more than 2000 times greater than that from the amide (k_1 (amide) = 4.36 x 10^{-4} $M^{-1}s^{-1}$, k_1(ester) = 9.8 x 10^{-1} $M^{-1}s^{-1}$ both at 25 °C). These results are also rationalised by the use of resonance theory. If the contribution from the amide resonance structure Z is greater than that of the ester resonance structure Z', the carbonyl carbon should be less electrophilic in an amide than in an ester. Thus, the rate constants for To^- formation support the prediction from resonance theory that the carbonyl carbon of the amide is less electrophilic, and thus more resistant to aqueous base-promoted hydrolysis, than that of the ester.

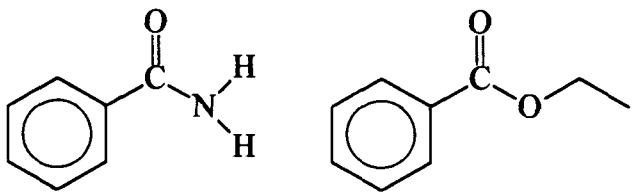

benzamide ethyl benzoate

Figure 7. Structures of benzamide and ethyl benzoate.

However, Wiberg and Laidig[9] have suggested that amide resonance does not exist. They claim that resonance theory predicts a reduced electron population at the nitrogen atom and a reduced C–N bond distance as the amide in Figure 8 rotates from the orthogonal conformation to the planar. According to their calculations, the electron population at the nitrogen atom *increases* as the amide in Figure 8 rotates from the orthogonal to the planar conformation, which is exactly opposite to that predicted by resonance theory. As for the C–O bond order, while the calculated amide C–O bond is slightly longer in the amide planar conformation relative to that in the orthogonal conformation, the change is small when compared with the change in the calculated C–N bond length for a planar and orthogonal amide.

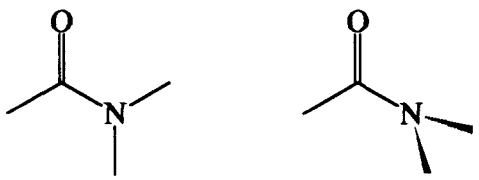

Planar amide 'Orthogonal' amide

Figure 8. Planar versus 'orthogonal' amides.

If resonance theory is no longer valid in light of the evidence from Wiberg and Laidig, is there an alternative theory that can replace resonance theory? From calculations by Wiberg and Laidig,[9] the amide nitrogen is sp^2 hybridised in the planar conformation, whereas it is sp^3 hybridised in the orthogonal conformation. In the planar conformation,

the lone pair in the p-orbital on N interacts with the LUMO of the amide ($n_N \rightarrow \pi^*(C–O)$, Figure 9), raising the energy of that LUMO relative to that in the orthogonal conformation. In the ground state, the planar conformation is normally preferred, and rotation about the C–N bond is associated with an energy barrier on the order of 15 kcal/mol. According to Wiberg and Laidig, the sp^2 hybridised nitrogen in the planar conformation is more electronegative than the sp^3 hybridised nitrogen of the orthogonal conformation. As a result, the nitrogen removes electron density from the carbonyl carbon making a more ionic and stronger C–N bond in the planar conformation.

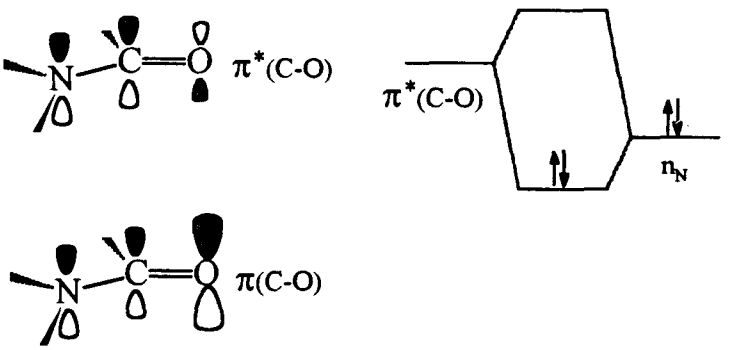

Figure 9. Interaction of the $\pi^*(C–O)$ and the n_N. Also shown are the $\pi^*(C–O)$, $\pi(C–O)$ molecular orbitals, and the n_N p-orbital.

1.3 Enzyme-Catalysed Hydrolysis of Amides

Currently, there are four known classes of proteases that can hydrolyse amides.[16] Three of these classes, the serine, thiol, and zinc proteases are active at pH 7. The general scheme for the enzyme-catalysed hydrolysis of an amide is outlined in Figure 10.

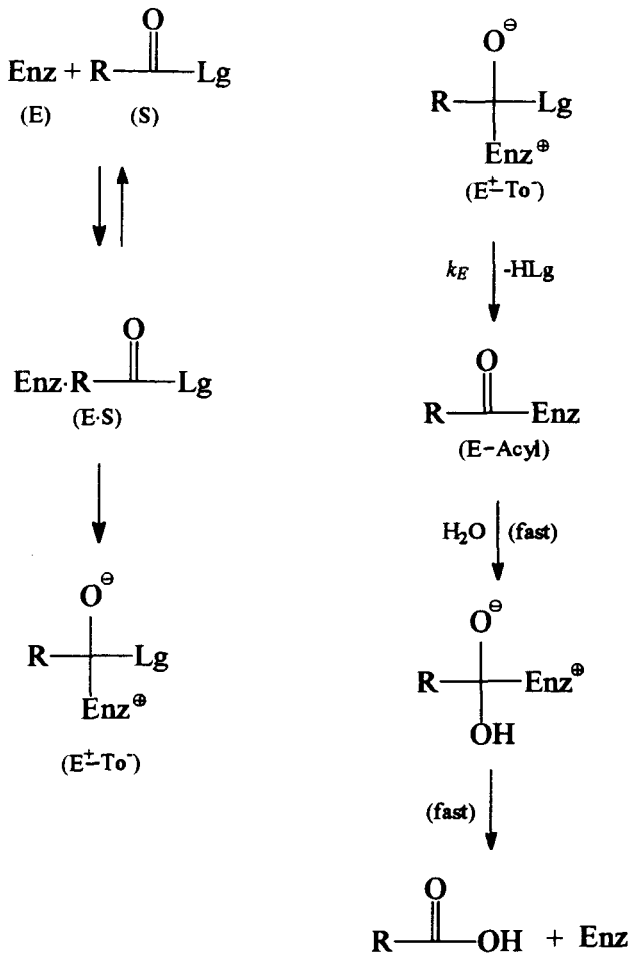

Figure 10. Scheme for enzyme-catalysed amide hydrolysis.

After an enzyme binds the polypeptide or protein, the amide linkage is attacked by a nucleophile from the enzyme to yield a tetrahedral intermediate formed with the enzyme (E^+–To^-). The E^+–To^- then proceeds to breakdown to the amine (HLg) and acylenzyme intermediate (E–Acyl). The reactivation of the enzyme is achieved by hydrolysis of the acylenzyme to the active enzyme and carboxylic acid. In general, this reactivation is fast relative to E–Acyl formation, so the rate constants for E–Acyl breakdown need not be considered here. The rate constant, k_{cat}/K_M, is the overall second-order rate constant for the formation of the E–Acyl. The k_{cat}/K_M for a serine-catalysed hydrolysis of a primary amide is on the order of 10^0 to 10^1 $M^{-1}s^{-1}$ at neutral pH,[16] whereas the rate of the

uncatalysed hydrolysis of a typical peptide bond is 10^{-11} $M^{-1}s^{-1}$.[17] Therefore, the overall enzymatic rate acceleration for an enzyme-catalysed amide hydrolysis is typically on the order of 10^{11}.

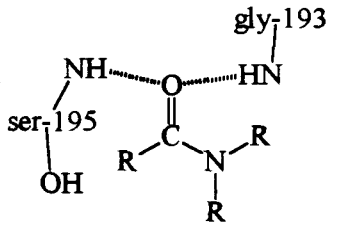

Figure 11. Hydrogen bonding with the enzyme and the carbonyl oxygen of an amide group.

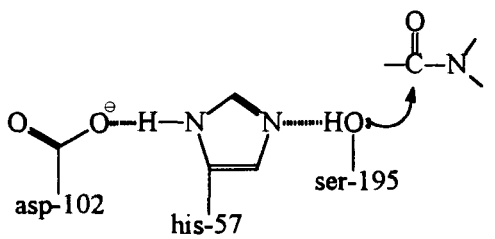

Figure 12. Catalytic triad of the serine proteases.

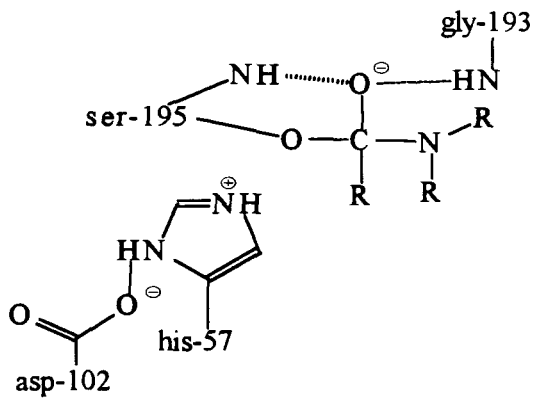

Figure 13. Tetrahedral intermediate formed with an enzyme.

The serine proteases require the two active site residues (Figure 11) to bind the amide group. These residues, ser-195 and gly-193, form hydrogen bonds to the amide carbonyl oxygen. This binding also increases the electrophilicity of the amide carbonyl carbon. The serine proteases also possess a catalytic triad made up of the three active site amino acid residues, ser-195, his-57, and asp-102. These three amino acid residues work together to form To^- in the enzyme in the manner shown in Figures 12 and 13. In the serine proteases, the $E^+–To^-$ is formed with ser-195.

1.4 The Scheme for Buffer-Promoted Hydrolysis in Aqueous Basic Media

Catalysis of amide hydrolysis by bases (B) other than hydroxide ions in aqueous media, also known as general-base catalysis, has been observed for a few amides.[4,18] The most notable example is the occurrence of general-base-catalysed To^- breakdown during the hydrolysis of some anilides.[18] However, no evidence was seen for general-base-catalysed To^- formation in these studies.

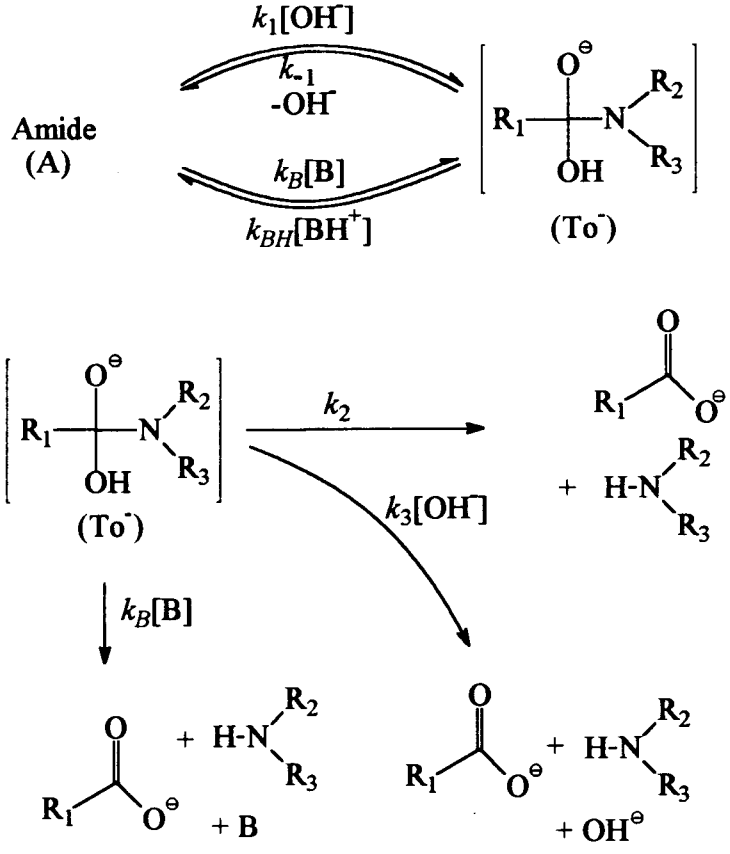

Figure 14. Scheme for hydroxide ion- and buffer-promoted amide hydrolysis.

The scheme for the hydroxide ion-promoted hydrolysis of amides is the same that described for the carboxylic acid derivatives given in Figure 4. The rate constants, k_1, k_{-1},

k_2, and k_3 for the hydroxide ion-promoted amide hydrolysis in Figure 14 replace k_A, k_{-A}, k_{E2}, and k_{E3}, respectively, (Figure 4) for the hydroxide ion-promoted hydrolysis of the CAD. In Figure 14, the basic buffer catalysis of To^- formation and breakdown in aqueous media is included in the scheme for aqueous base-promoted hydrolysis. The basic buffer species and a water molecule promote To^- formation at the rate k_B[A][B], where k_B is a second-order rate constant, [A] is the concentration of the amide and [B] is the concentration of the basic buffer species. A water molecule is required for the buffer-promoted To^- formation, but as the concentration of water is scarcely affected by the hydrolysis reaction, it remains constant (55 M) and may be incorporated into k_B. Because To^- formation is reversible, the reverse process must involve the acidic-buffer-promoted To^- reversion to the amide at the rate $k_{BH}[To^-][BH^+]$, where k_{BH} is a second-order rate constant, and $[BH^+]$ is the concentration of the acidic buffer species. The breakdown of To^- to the products may be assisted by the basic buffer species at the rate k_{BP}[B], where k_{BP} is a second-order rate constant. Where buffer-promoted hydrolysis of an amide is observed, normally only the basic buffer species is considered for To^- formation. Sometimes, for To^- breakdown, promotion by both the acidic and the basic buffer species can be considered, but the promotion by the acidic buffer for To^- breakdown is neglected in the present scheme. The rate constant for the hydroxide ion- and buffer-promoted hydrolysis, k_{hyd} is derived from $\upsilon = k_{obs}^{hyd}[A]$ where υ (in Ms^{-1}) is the rate of the amide hydrolysis. By applying the steady-state approximation to To^-, k_{hyd} for hydroxide ion- and buffer-promoted hydrolysis may be derived to give Equation 1.

$$k_{hyd} = \frac{(k_1[OH^-] + k_B[B])(k_2 + k_{BP}[B] + k_3[OH^-])}{(k_{-1} + K'k_{BH}[B] + k_2 + k_{BP}[B] + k_3[OH^-])} \quad \textbf{(1)}$$

$$K' = \frac{[BH^+]}{[B]}$$

1.5 The Observation of *Carbonyl*-^{18}O Exchange During Hydrolysis

Where a tetrahedral intermediate such as To$^-$ is encountered along the hydrolytic pathway, the occurrence of *carbonyl*-^{18}O exchange often accompanies the hydrolysis. The *carbonyl*-^{18}O exchange allows a direct estimate of To$^-$ partitioning that is not obtainable from the hydrolysis experiments alone.[7,8,19] To$^-$ partitioning is the ratio of the sum of the rate constants for To$^-$ reversion that lead to the amide to the sum of the rate constants for To$^-$ breakdown that lead to the products.

A typical experiment for the observation of *carbonyl*-^{18}O exchange involves the use of *carbonyl*-^{18}O enriched amide. The labelled amide is then subjected to hydrolytic conditions for a period of time corresponding to one or two reaction half-lives of hydrolysis, after which the remaining amide is extracted and the *carbonyl*-^{18}O content is determined. If the percentage *carbonyl*-^{18}O is observed to have decreased during the hydrolysis, ^{16}O from the solvent must have exchanged with the original ^{18}O of the amide. When exchange is observed, it is evidence for an intermediate that is capable of such exchange and must have the following properties: (a) the ^{16}O is incorporated into the tetrahedral intermediate (To$^-$), (b) that the C–^{16}O and C–^{18}O bonds at To$^-$ are made to be equivalent for To$^-$ reversion to amide by either a symmetry element or rapid equilibrium, and (c) the life-time of the tetrahedral intermediate is finite and greater than the time necessary for the exchange process.

The scheme for ^{18}O exchange, which includes the terms for the buffer-promoted exchange, is given in Figure 15. The derived rate constant for the *carbonyl*-^{18}O exchange (Equation 2) is calculated from the overall rate of To$^-$ reversion to the amide ($v = -k_{ex}[To^-] = k_{-1}[To^-] + k_{BH}[To^-]$). The steady-state approximation is also applied to [To$^-$]. In this way, exchange refers to the reversal of the To$^-$ to starting materials. The value, 2, in the expressions for exchange arises from the derived rate constant because

only half of the To⁻ reversion to amide is associated with the loss of ^{18}O. The full equation for the buffer-promoted To⁻ partitioning, k_{ex}/k_{hyd} is given in Equation 3.

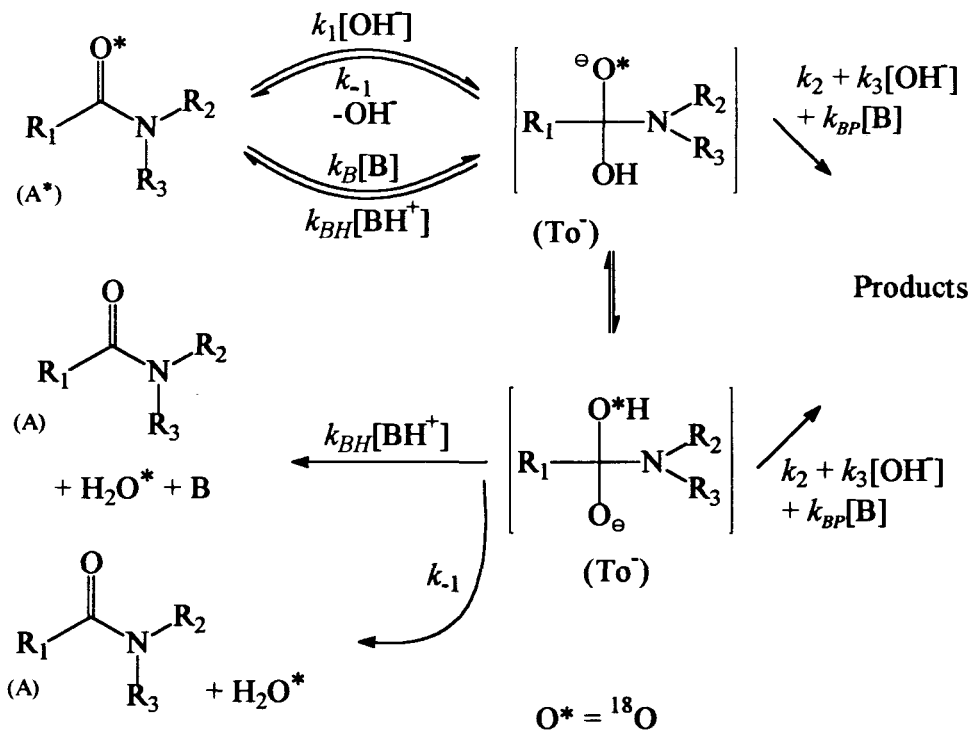

Figure 15. Scheme for the *carbonyl*-^{18}O exchange that accompanies hydroxide ion- and buffer-promoted hydrolysis of an amide. The breakdown of To⁻ to the products follows the same pathways shown in Figure 1 for To⁻ breakdown to the products.

$$k_{ex} = \frac{(k_{-1}+k_{BH}K'[B])(k_1[OH^-]+k_B[B])}{2(k_{-1}+k_{BH}K'[B]+k_2+k_{BP}[B]+k_3[OH^-])} \quad (2)$$

$$\frac{k_{ex}}{k_{hyd}} = \frac{k_{-1}+k_{BH}K'[B]}{2(k_2+k_{BP}[B]+k_3[OH^-])} \quad (3)$$

Two assumptions[19] must hold true for Equation 3 to be valid. The first is the assumption that the intermediate that allows exchange must also lie on the hydrolytic pathway for amide hydrolysis. The second is that the protonic equilibration between ^{16}O

and ^{18}O (Figure 15) is rapid when compared with the other reactions of To^-. Neither of these assumptions appears unreasonable, and ^{18}O exchange evidence from the similar amide **2**[19] suggests that these assumptions should also be valid for amide **1**. (See Figure 21 for structures of **1** and **2**).

The To^- partitioning identifies which transition state (that for To^- formation or for To^- breakdown) is rate limiting (see Figures 16, 17, and 18). The reaction coordinate in each figure is a 'slice' from the total energy surface for the aqueous base-promoted hydrolysis of an amide. This 'slice' is taken along the lowest energy path that leads to hydrolysis. Once the To^- is formed, it may either revert to the amide or breakdown to form the products. The overall energy that is required for To^- to revert to the amide via the reaction steps in Figure 14 can be represented by the energy barrier preceding the To^- in Figures 16, 17, and 18. The overall energy that is required for To^- to breakdown to the products can be represented by the energy barrier following To^-, also in Figures 16, 17, and 18. In Figure 16, the energy of each barrier is the same and To^- partitioning favours the reversion to the amide and the breakdown to the products equally, and $k_{ex}/k_{hyd} = 0.5$. In Figure 17, the overall energy required for To^- reversion is greater than that for breakdown to products. Therefore, To^- breakdown to the products is more frequent than the reversion to the amide, and $k_{ex}/k_{hyd} < 0.5$. A similar argument may be made for the case in Figure 18 where To^- partitioning favours the reversion to amide.

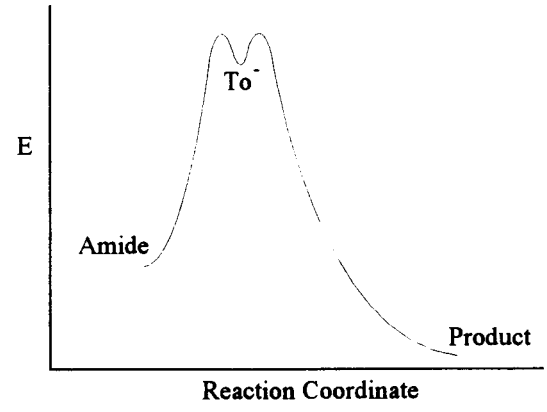

$$\frac{k_{ex}}{k_{hyd}} = 0.5$$

Figure 16. Energy versus reaction coordinate for which equal To^- partitioning is observed.

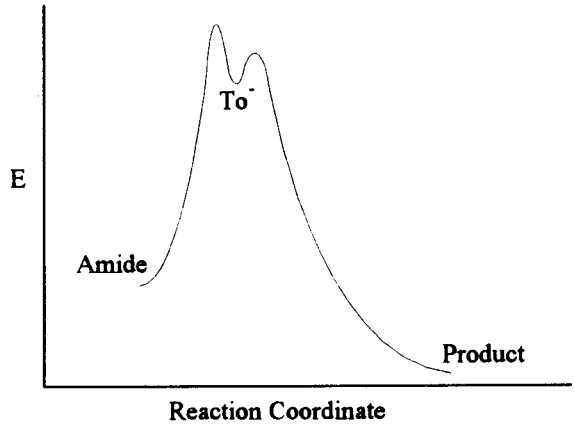

$$\frac{k_{ex}}{k_{hyd}} < 0.5$$

Figure 17. Energy versus reaction coordinate for which To^- partitioning favours product formation from To^-.

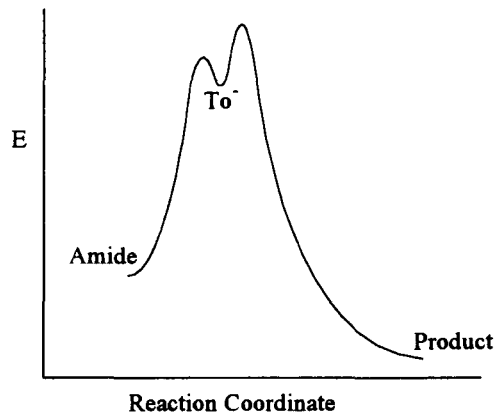

$$\frac{k_{ex}}{k_{hyd}} > 0.5$$

Figure 18. Energy versus reaction coordinate for which To^- partitioning favours To^- reversion to amide.

The observation of *carbonyl*-^{18}O exchange allows the elucidation of trends in the hydrolysis of amides. A group of representative amides is given in Table I along with the corresponding values for k_{obs}^{hyd}, k_{ex}/k_{hyd}, and pK_a of the protonated free amine portion. The general trends that dictate the rates for hydroxide ion-promoted hydrolysis of amides are related to the basicity of the nitrogen on the Lg, the carbonyl carbon electrophilicity, and the steric bulk of the amide.[20]

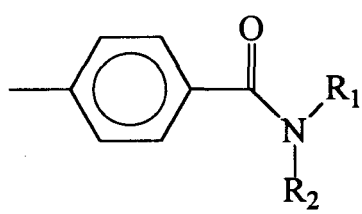

3a $R_1 = R_2 = -CH_2CF_2CF_2CH_2-$
3b $R_1 = CH_2CH_3$, $R_2 = CH_2CF_3$
3c $R_1 = R_2 = -(CH_2)_2O(CH_2)_2-$
3d $R_1 = R_2 = CH_3$

Figure 19. Representative amides from reference 8.

Table I. The hydroxide ion-promoted hydrolysis rate constants[a,b] and the corresponding To$^-$ partitioning for various amides (25 °C, μ = 1.00 M (KCl)), and pKa of conjugate of the amine leaving groups.

amide	T (°C)	k_{hyd} ($M^{-1}s^{-1}$) 10^3	k_{ex}/k_{hyd}	pK_a ($H_2N^+R_1R_2$) 25 °C
2[c]	25	1290	0.24	<-3.8
3a[c]	73	2.47	9	4.05
3b	100	0.0313	32	6.3
3c	72	0.879	0.13	8.33
3d	100	1.15	0.01	10.64

[a] For reactions first-order in hydroxide ion concentration.
[b] Reference 19.
[c] From data below pH regions where second-order terms in hydroxide ion concentration are observed.

The mechanism for To$^-$ partitioning during the aqueous base-promoted hydrolysis of amides is currently interpreted in terms of the nitrogen basicity on the Lg.[8] When the nitrogen basicity of the Lg is high, as in **3c–d**, To$^-$ partitioning favours To$^-$ breakdown to the products, which requires that the rate limiting step for the hydrolysis of tertiary amides be To$^-$ formation. The observed SKIEs[21] are consistent with nitrogen protonation prior to the Lg departure (pathway (*a*) in Figure 20), so that the C–N cleavage during To$^-$ breakdown produces the amine rather than the amido group. As the nitrogen basicity of the Lg drops (e.g., **3b**), To$^-$ partitioning favours To$^-$ reversion to the amide, and requires that To$^-$ breakdown to the product be rate limiting. This change in the rate limiting step is interpreted as a result of the reduced nitrogen basicity so that the nitrogen cannot be protonated so easily prior to C–N cleavage. When amine basicity drops further (e.g., **3a**), the N can no longer be protonated prior to C–N cleavage (pathway (*b*) in Figure 20), and To$^-$ breakdown is rate limiting. However, the amine portion also has a better ability to leave as its anion due to its decreased basicity, and does not require the protonation of the

nitrogen prior to C–N cleavage. While the rate limiting step remains To$^-$ breakdown for **3a**, further drops in the amine basicity (e.g., **2**) result in the To$^-$ partitioning favouring products again, and To$^-$ formation becomes rate-limiting.

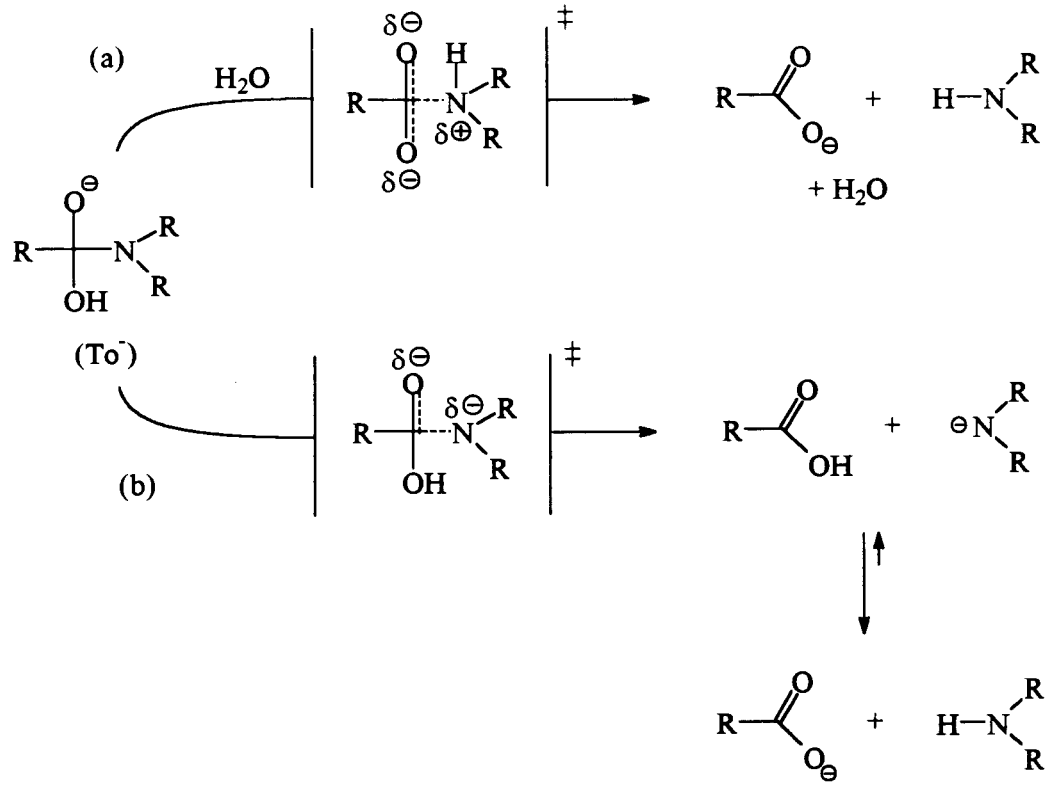

Figure 20. Breakdown of tetrahedral intermediate, To$^-$. In route (a), nitrogen is protonated prior to C–N cleavage, whereas in route (b), nitrogen is protonated subsequent to C–N cleavage.

1.6 Deuterium Solvent Kinetic Isotope Effects (SKIE)

The comparison of observed and estimated SKIEs have been useful in distinguishing between mechanistic alternatives.[22] The expected solvent isotope effect for a particular mechanism may be estimated by means of Equation 8, which makes use of fractionation factors, Φ.[23] While agreement between the expected and measured effects does not prove that a particular mechanistic pathway is correct, differences between an expected effect and the observed effect may show that a particular pathway is inconsistent with the SKIE.

The SKIE arises from a change in the vibrational energy levels of a C–H and a C–D bond.[5] The vibrational frequencies of a C–L bond (L = H or D), given by ν (cm^{-1}), are inversely proportional to the square root of their reduced masses, given by μ_L (g) (Equation 4).

$$\frac{\nu_H}{\nu_D} = \frac{(f_H/\mu_H)^{1/2}}{(f_D/\mu_D)^{1/2}} \quad (4)$$

ν_L = vibrational frequency
μ_L = reduced mass of the two groups attached to the bond. L = H or D.
f_L = force constant

The force constants, f_H and f_D for any particular C–L bond are assumed to be equal, so that the relative vibrational frequencies become equivalent to the square root of the ratio of their reduced masses. During the course of a reaction, the force constants of the C–L bonds change. Because the force constants for any particular C–L bond may be considered equal, the change in the vibrational energy level due to the C–H bond changes more than that due to a C–D bond. The vibrational energy levels, E_{Vi}, may be calculated from the vibrational frequency by the use of Equation 5.

$$E_{vi} = (V+1/2)h\nu_{H,D} \quad (5)$$

$$V = 1, 2,...$$

V is vibrational quantum number.

$$AH + SD \leftrightharpoons AD + SH \quad (6)$$

$$\Phi = \frac{[AD][SH]}{[AH][SD]}$$

A = solute molecule
S = solvent molecule

Deuterium accumulates at sites that will result in larger force constants, because C–D bonds generally result in a reduced E_{vi}. The ratio of deuterium to protium at any hydrogenic site (AD/AH) in Equation 6 may be different from that of water (SD/SH). The fractionation factor, Φ, reflects this difference as the equilibrium isotope effect a reaction such as that in Equation 6. In general, fractionation factors obey the functional-group rule. For example, all alkoxides have approximately the same fractionation factor, 0.74. A list of the important fractionation factors[5] used in the estimation of the SKIE for amide hydrolysis are listed in Table II.

Table II. List of fractionation factors for each functional group commonly encountered in amide hydrolysis.

Functional Group	Fractionation Factor
$R–O^{-}\cdots L–OR$	0.70 (hydroxide); 0.74 (methoxide)
$R_3C–L$	1
$R_3N^{+}–L$	1
RO–L	1
$^{-}O–L$	1.25

$$\frac{K_D}{K_H} = \frac{\Pi\Phi_P}{\Pi\Phi_R} \tag{7}$$

$$\frac{k_D}{k_H} = \frac{\Pi\Phi_{TS}}{\Pi\Phi_R} \tag{8}$$

$$\Phi_{TS} = (\Phi_P)^{\alpha}(\Phi_R)^{(1-\alpha)} \quad (9)$$

α = Position of transition state along reaction coordinate.

These fractionation factors can be used to estimate equilibrium isotope effects as K_D/K_H, which are defined in Equation 7. The Φ_R and Φ_P are the fractionation factors for the reactant and product hydrogenic sites, respectively. By estimating the Φ_{TS} by means of Equation 9, the SKIE can be similarly estimated by using Equation 8 because, according to transition-state theory, the transition state is considered to be in equilibrium with reactants. Therefore, the kinetic isotope effect can be estimated from fractionation factors for the transition state and the reactants. Because the interactions involving deuterium and protium in the transition state are not complete bonds, they must be calculated by means of Equation 9. The transition state is treated as close to a tetrahedral species, being 70 percent along the reaction coordinate for To^- formation. The fractionation factors for the transition state are then estimated by using Equation 9. Fractionation factors for protons 'in flight' cannot be treated in this way. A proton transferring between electronegative atoms (such as O and N) at the transition state has a fractionation factor value of around 0.5,[23] although this number often varies between 0.3 and 0.5.[23]

1.7 Activated Amides

The neutral hydrolysis of any of the common peptides is too slow to allow an extended study of the hydrolysis rate constants. As a result, the hydrolysis of amides is almost always observed in aqueous-acidic or basic media, which promotes the reaction so that rate constants can be estimated within a reasonable period of time. In addition to enhancing the rate of amide hydrolysis by means of acid or base promotion, the reactivity of an amide itself may be enhanced by the substitution of strongly electron withdrawing

groups for the alkyl groups on the amide. Commonly, activated amides contain strong electron withdrawing groups that can remove electron density from the C–N bond (Figure 21). Acyl substituent effects[24] demonstrate how electron withdrawing groups in the acyl portion also increase the reactivity of the amide for hydrolysis. The rate for To^- formation (k_1) from an amide such as trichloroacetanilide is more than 300 times faster than that of chloroacetanilide. Similar effects are reported when electron density is removed from the C–N bond by means of resonance effects from within the amido group.[25]

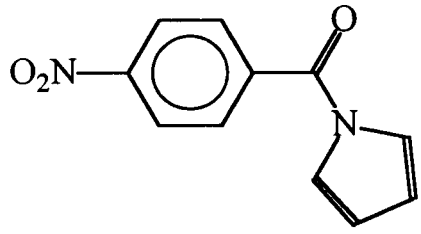

N-p-nitrobenzoylpyrrole

1

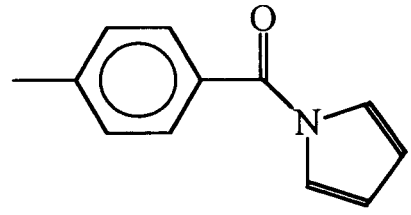

N-toluoylpyrrole

2

Figure 21. Two activated amides.

When amide hydrolysis occurs in vitro at pH = 7, the extrapolated reaction half-lives can range from a few days for reactive amides[19] to hundreds of years for the less reactive amides.[7] The observed pseudo first order hydrolysis rate constant for the hydroxide ion-promoted hydrolysis of benzamide at pH = 7 is calculated from $k_{obs}^{hyd} = k_1[OH^-]$. The resulting second-order rate constant, k_1, is 4.4×10^{-11} s^{-1}, which corresponds to a reaction half-life of about 500 years. By the use of radioactive labelling techniques, Kahne and Still[17] measured the hydrolysis rate at T = 25°C of the Phe–Gly bond in (L)Phe(L)Phe(L)PheGlyOH in neutral aqueous media. The observed pseudo first order hydrolysis rate constant for this hydrolysis is 3×10^{-9} s^{-1}, which corresponds to a half-life of 7 years. Between pH = 6 and 8, the hydrolysis rate was observed to be nearly independent of pH, which is consistent with a reaction transition state containing only amide and water. Therefore, at pH 7, this reaction is considered to be an example of uncatalysed amide hydrolysis. The corresponding second-order rate constant, k_1, for the

uncatalysed hydrolysis of a peptide C–N bond (where the rate of hydrolysis is $k_1[H_2O][A]$, and $[H_2O]$ = 55 M) is 5 x 10^{-11} $M^{-1}s^{-1}$. Most conventional analytical methods cannot detect parts per million or parts per billion concentrations of hydrolysis products formed during such a hydrolysis experiment. Therefore, chemists must resort to the acid- or base-catalysed hydrolyses of amides, and the study of activated amides.

1.8 Occurrence of Buffer Catalysis

Buffer catalysis has been frequently reported during the hydrolysis of various anilides.[26] Eriksson provided support for the general-base-catalysed To^- breakdown during the buffer-catalysed hydrolysis of trifluoro- and trichloroacetanilide. Although their scheme did not explicitly show any regeneration of the basic buffer species (required if the strict definition of catalysis is to be upheld), a final proton transfer from the acidic buffer species to the free amine anion would form the free amine and regenerate the basic buffer species.

Buffer catalysis was observed by Menger and Donohue[4] during the aqueous base-promoted hydrolysis of **1** in the presence of added diazabicyclooctane (DABCO), and trimethylamine (TMA), and carbonate buffer. A scheme involving buffer-catalysed To^- formation was proposed.[4] The derived expression in Equation 1, according to the scheme for the buffer-promoted hydrolysis of **1**, is not necessarily a linear function of the basic buffer species, even assuming that $k_{BP} = 0$. Many of Menger and Donohue's plots of the k_{obs}^{hyd} versus the total buffer concentration were either curved concave downwards or greatly scattered, and yet the plots were analysed according to a linear model. It is entirely possible that Menger and Donohue did not have sufficient data to allow a fit to any nonlinear function. However, no expression for the buffer-promoted hydrolysis of **1** was derived according to the scheme proposed in the previous work.

A possible cause for the observed curvature in Menger and Donohue's plots of the k_{obs}^{hyd} versus the total buffer concentration is the lack of ionic strength control in their study. Any reaction that involves charged intermediates or transition states is often affected by the ionic strength. The scheme in Figure 14 definitely involves the charged intermediate, To^-, and probably involves charged transition states as well.

Menger and Donohue's conclusion that the To^- formation from **1** was probably subject to general-base catalysis was based solely on a large primary solvent isotope effect, $k_{HOH}/k_{DOD} = 4.1$ at pH=9.4. However, full details of the measurement and calculation of this SKIE were not given.[4] Furthermore, this value included a correction, which was not described in detail. A large SKIE is normally associated with a proton 'in flight', but does not conclude that general-base catalysis occurs. Also, according to the scheme in Figure 14, the basic buffer species is not regenerated overall during the hydrolysis of **1**. Because catalysis requires that the catalyst be regenerated within the scheme, the term 'catalysis' cannot be strictly applied to this scheme.

What follows is an investigation into the hydroxide ion- and buffer-promoted hydrolysis of **1** under more strictly controlled conditions, especially the control of ionic strength. The results of k_{obs}^{hyd} will be analysed according to the derived expression for hydrolysis, given by Equation 1. Support will be given for the scheme as presented in Figure 14. With the combination of the observed pseudo first order hydrolysis and exchange rate constants, To^- partitioning will be determined, and the effect of a buffer during the aqueous base-promoted hydrolysis of **1** can be assessed.

The aqueous base-promoted hydrolysis of **1** is investigated under conditions as similar as possible to the original investigation by Menger and Donohue. In this way, the remaining ambiguities for the hydrolysis of **1** in the presence of added DABCO and TMA can be clarified. The only intentional experimental difference between this and the previous work that may produce differing observations is the control of ionic strength. By

ensuring that the concentration of salt[27] in the solution be constant at 1.00 M (maintained with KCl), the effect of ionic strength on the rate of hydrolysis will also be constant.

The present work also investigates To^- partitioning with the use of *carbonyl*-^{18}O exchange to measure the exchange rate constants during the hydrolysis of **1**. To^- partitioning at zero added buffer identifies the rate limiting step, which subsequently identifies the step that is promoted by the buffer. The dependence of the To^- partitioning on the added buffer identifies whether only one step is promoted (either To^- reversion to amide or breakdown to products), or if both steps (To^- reversion and breakdown) are promoted. In addition to identifying the step or steps that are promoted by the buffer, the present work also identifies the form of promotion, either by the basic or the acidic buffer species. Once the form of promotion is identified, transition states can be proposed for To^- formation and breakdown.

Chapter 2

Experimental

2.1 Instrumentation

2.1.1 Instruments for Identification of Materials

The following instruments were used for the identification of the materials synthesised in this research:

NMR

All of the ^{1}H NMR and ^{13}C NMR spectra were obtained with the use of a Bruker AMX400 NMR spectrophotometer with an operating frequency of 400.13 MHz for ^{1}H and 100.61 for ^{13}C.

Mass Spectrometry

The mass spectra were obtained by the use of a Hewlett Packard 5985 Mass Spectrometer, using direct insertion and electron impact ionisation (70 eV). The m/z ratio was observed between 40 and 500 m/z, although the spectra were plotted between 40 and 230 m/z. The absolute abundances of $M^{\cdot+}$ and $M^{\cdot+} + 2$ (m/z = 216 and 218) were used to calculate the percentage *carbonyl*-^{18}O content for the calculation of observed pseudo first order exchange rate constants for the hydrolysis of **1**.

Microanalysis

The results for microanalysis were obtained by M. Yang at the Simon Fraser University Microanalysis Laboratory.

pH measurements

The pH of buffer solutions was measured with the use of a Radiometer PHM82 standard pH meter and a Broadley-James combination electrode (silver/silver chloride reference). A Radiometer TTT80 titrator assembly along with a Radiometer ABU80 autoburette apparatus maintained the pH at the desired level when necessary.

X-ray

The data for the structural determination of **1** were collected at 205 K with the use of an Enraf Nonius CAD4F diffractometer equipped with an in-house modified low-temperature attachment, and using graphite monochromatised Mo K_{α} radiation.

2.1.2 Instruments for Kinetic Observations

The concomitant absorbance change during the hydrolysis of **1** permits the calculation of the observed pseudo first order hydrolysis rate constants and is observed with the use of either UV spectroscopy or stopped-flow combined with UV spectroscopy. The decrease in the percentage ^{18}O content decrease that accompanies the hydrolysis of **1** permits the calculation of observed pseudo first order exchange rate constants for the hydrolysis of **1** and is observed with the use of mass spectrometry.

UV Spectroscopy

The absorbance versus time data were obtained with the use of a Cary 3E UV-vis spectrophotometer. Quartz cuvettes (path length = 1 cm) were used, and the temperature of the solution inside the cuvette was maintained at 25.0 ± 0.1 °C with the use of a Cary Thermostattable multicell block. Although UV-vis spectroscopy permits the collection of accurate absorbance versus time data for reactions that have half-lives on the order of seconds, the shortest reaction half-life observed by the use of this method was 1.9 min.

Stopped flow

For faster reactions associated with half-lives on the order of milliseconds, a DURRUM 110 stopped flow apparatus was used to measure the absorbance versus time data for the calculation of the observed pseudo first order hydrolysis rate constants for amide hydrolysis. The temperature of each solution in the drive syringes of the stopped-flow apparatus was maintained at 25.0 ± 0.1 °C with the use of a Lauda RM6 circulating water bath. The observation of the UV absorbance change in conjunction with the stopped flow method allows the determination of half-lives as short as 5 ms. The shortest half-life determined by the use of this method for this research project was 33 ms.

Syringe pump apparatus

This apparatus (Figure 22) consists of a Orion Sage syringe pump (model 355), a Lauda RM6 temperature controlled circulating water bath and Teflon tubing (inner diameter = 1/16") and a Radiometer TTT80 titrator assembly attached to a Radiometer ABU80 autoburette apparatus. The circulating water bath was used to maintain the temperature of the solutions inside the tubing at 25.0 ± 0.1 °C. The tubing consists of two short tubes (1 m each, in length) to allow the equilibration of each reactant solution to 25 °C, and one long tube (3 m in length) in which the hydrolysis occurs. Each syringe is connected to one short tube with the use of Luer fittings. The remaining ends of the short tubes are connected to the long tube by means of a three-way connector. In this way, as the syringes are emptied with the use of the syringe pump, the two solutions are expelled into the short tubes where the temperatures of the solutions equilibrate to 25 °C. The two solutions mix at the three-way connector, whereupon hydrolysis commences in the long tube. The hydrolytic solution then elutes into a vessel where the pH is maintained at 4 by the use of the titrator assembly along with the autoburette apparatus.

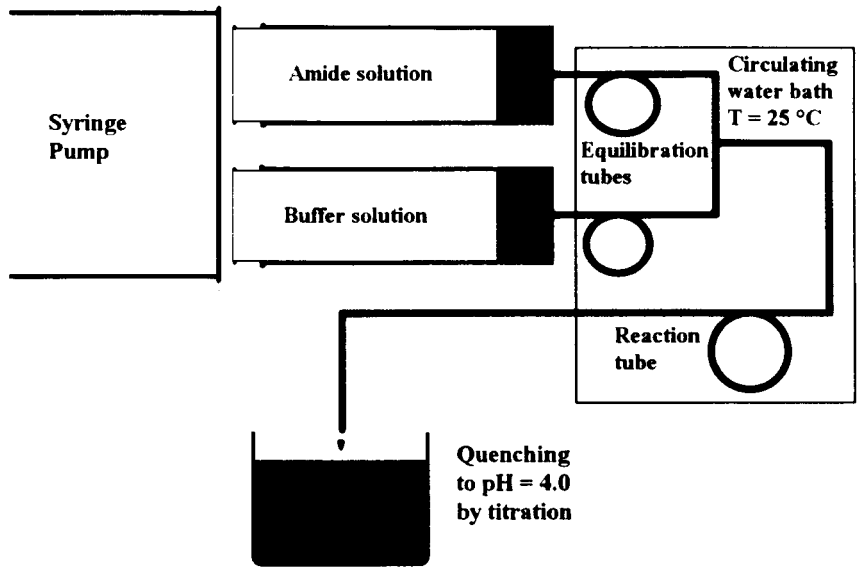

Figure 22. Apparatus for the determination of observed pseudo first order exchange rate constants.

2.2 Synthesis

2.2.1 Materials

The following materials were purchased from commercial sources and used in the synthesis of **1**, *carbonyl*-^{18}O labelled **1**, and in the preparation of trimethylamine (TMA) and 1,4-diazabicyclo[2.2.2]octane (DABCO) buffers, and aqueous basic solutions. All materials were used without further purification unless stated otherwise.

Pyrrole (Aldrich, purified by the use of distillation under a dry nitrogen atmosphere at ambient pressure immediately prior to use), *p*-nitrobenzoyl chloride (Lancaster), potassium metal (Anachemia, washed with and stored in hexane to remove mineral oils from the metal surface immediately prior to use), thionyl chloride (Anachemia), ^{18}O-labelled water (Isotec, 98.5 atom % ^{18}O, lot #DU2255, $H_2{}^{18}O$), 1,4-diazabicyclo[2.2.2]octane (Aldrich, 98 %, DABCO), trimethylamine hydrochloride (SIGMA, TMA hydrochloride), hydrochloric acid (BDH, 1 M and 0.1 M, HCl), benzoyl chloride (BDH), deuterium oxide

(Isotec, 99.9 atom % D, D_2O), potassium chloride (BDH, KCl), potassium hydroxide (Anachemia, KOH), sodium hydroxide (BDH, NaOH), diethyl ether (BDH), hexane (BDH), isobutanol (Caledon), reagent grade tetrahydrofuran (BDH, dried over sodium and distilled under a dry nitrogen atmosphere at ambient pressure, THF), reagent grade toluene (BDH, dried over calcium hydride, and distilled under a dry nitrogen atmosphere at ambient pressure).

2.2.2 *N*-*p*-nitrobenzoylpyrrole (1)

All steps in the synthesis of **1** were performed under a dry nitrogen atmosphere, up to the addition of the water/diethyl ether mixture. Small portions of potassium metal (0.9 g, 23.13 mmol, washed in hexane) were added to a solution of distilled pyrrole (1.60 mL, 23.13 mmol) and freshly distilled anhydrous THF (20 mL). The solution was heated to reflux until no potassium metal remained. The solution was cooled to ambient temperature, and freshly distilled anhydrous toluene (70 mL) was added. Distilled anhydrous toluene (200 mL) containing *p*-nitrobenzoyl chloride (4.29 g, 23.13 mmol) was added in a dropwise manner to the solution, heated to reflux for 24 h, and then cooled to ambient temperature. A mixture of 1:1 ice-cold water/diethyl ether (total volume 100 mL) was then added to the solution and vigorously mixed. The aqueous layer was removed, leaving the diethyl ether layer. The diethyl ether layer was washed with ice-cold water (50 mL), which was removed as before and combined with the first aqueous layer. Fresh diethyl ether was added to the combined aqueous layers and vigorously mixed. The aqueous layer was removed and all of the ether layers were combined. The ether was evaporated to dryness by the use of rotary evaporation under reduced pressure. The resulting black residue was heated to 100 °C at 0.25 mtorr, causing the product **1** to sublime onto a cold finger. The product **1** was further purified by the use of recrystallisation from hexane/isobutanol (1:30).

Yield 25 %: m.p. 128.5-130°C (lit.[4] 127-128 °C).

^{1}H NMR ($CD_3C(O)CD_3$): δ 6.40 (dd, 2H, $J_{10,9} = J_{10,12}$ = 2.4 Hz, H-10, H-11), 7.29 (dd, 2H, $J_{9,10} = J_{9,11}$ = 2.4 Hz, H-9, H-12), 8.04 (d, 2H, $J_{1,2}$ = 8.9 Hz, H-1, H-6), 8.43 (d, 2H, $J_{2,1}$ = 8.9 Hz, H-2, H-5). (See Figure 32 for numbering system).

$^{13}C\{^1H\}$ NMR ($CD_3C(O)CD_3$): δ 114.52 (C-10, C-11), 121.97 (C-9, C-12), 124.59 (C-1, C-6), 131.36 (C-2, C-5), 140.04 (C-8), 150.93 (C-7), 166.63 (C-3).

Mass Spec. m/z, (intensity): 216 (65), 150 (100), 120 (20), 104 (25), 92 (21), 76 (23).

Anal. Calculated for $C_{11}H_8N_2O_3$: C, 61.11; H, 3.73; N, 12.95. Found: C, 61.30; H, 3.69; N, 12.97.

IR, KBr pellet, cm^{-1} (intensity): 3155 (w), 3107 (w), 1692 (s), 1601 (m), 1519 (s), 1474 (s), 1409 (s), 1332 (s), 1256 (w), 1189 (w), 1112 (w), 1091 (m), 1075 (m), 1037 (w), 1012 (m), 972 (m), 884 (m), 865 (m), 844 (s), 747 (s), 730 (s) 712 (s).

2.2.3 *p*-Nitro-*carbonyl*-^{18}O-benzoyl chloride[28]

Prior to its use, *p*-nitrobenzoyl chloride was purified by distillation (5 mtorr, 125 °C). The purified *p*-nitrobenzoyl chloride (1.33 g, 7.17 mmol) was added to freshly distilled anhydrous THF (15 mL) under a nitrogen atmoshpere. The ^{18}O-labelled water (129 μL, 7.17 mmol) was added and the solution stirred at ambient temperature for 24 h. The solvent was evaporated to dryness by the use of rotary evaporation under reduced pressure. Freshly distilled anhydrous toluene (15 mL) was added to the dried residue followed by the dropwise addition of thionyl chloride (1.04 mL, 14.34 mmol). The mixture was heated to reflux for 18 h. The solvent was removed under reduced pressure as before and the dry residue was purified by the use of distillation (5 mtorr, 125 °C).

2.2.4 *N*-*p*-nitro-*carbonyl*-^{18}O-benzoylpyrrole (^{18}O-1)

N-*p*-nitro-*carbonyl*-^{18}O-benzoylpyrrole (^{18}O-**1**) was prepared analogously to the preparation of **1**, except *p*-nitro-*carbonyl*-^{18}O-benzoyl chloride is used.

Overall yield (from *p*-nitrobenzoyl chloride): 21 %.

Mass Spec. m/z (intensity): 218 (59), 216 (72), 152 (68), 150 (100), 122 (11), 120 (11), 106 (21), 104 (30), 94 (16), 92 (17), 76 (44).

IR, KBr pellet, cm^{-1} (intensity): 3155 (w), 3107 (w), 1692 (s), 1660 (s), 1601 (m), 1519 (s), 1474 (s), 1409 (s), 1332 (s), 1256 (w), 1189 (w), 1112 (w), 1091 (m), 1075 (m), 1037 (w), 1012 (m), 972 (m), 884 (m), 865 (m), 844 (s), 747 (s), 730 (s) 712 (s).

2.3 Preparation of Buffers

Buffer systems of TMA or DABCO were prepared in the following manner:

2.3.1 Preparation of TMA Buffers for Hydrolysis

A stock solution of aqueous TMA hydrochloride salt (1.00 M, 250.0 mL) was prepared by dissolving TMA hydrochloride salt (23.893 g) in water (250.0 mL). A stock solution of potassium chloride (KCl, 1.00 M, 1.0 L) was prepared by dissolving KCl (74.543 g) in water (1.0 L), and a stock solution of potassium hydroxide (KOH, 1M approx., 500 mL) was prepared by dissolving KOH (33 g) in water (500 mL). All stock solutions were passed through a sintered-glass filter to remove any dust particles. The hydroxide ion concentration was determined by the use of titration with aqueous hydrochloric acid (HCl, 0.100 M). An appropriate volume of the aqueous KOH solution (1.0 M) was added to a portion of the stock aqueous TMA hydrochloride (23.0 mL, 1.00 M) according to Table III. The resulting buffer solution was then diluted to a total volume of 100 mL with aqueous KCl (1.00 M). (When the total concentration of salt (KCl) is 1.00 M at 25 °C in the final solution, the ionic strength of the solution is approximately 1.00. In accordance with the current literature,[8] the concentration of the salt that maintains ionic strength is expressed as μ = 1.0 M (KCl)). The pH of the solution was then measured.

Table III. Volume of KOH added to aqueous TMA to obtain given pH.

Buffer pH[a]	volume of KOH (1.012 M) added (mL)	quantity KOH (moles)
10.55	14.06	0.0142
10.18	10.00	0.0101
9.76	5.18	0.00524
9.41	2.76	0.00279
9.11	1.47	0.00149

[a]Measured values

The resulting 0.230 M buffer solutions in Table III were diluted with stock KCl (1.00 M) to give total buffer concentrations of 0.230, 0.184, 0.138, 0.092, and 0.046 M. These solutions were used as the aqueous media for the determination of the observed pseudo first order hydrolysis rate constants for the hydrolysis of **1** in TMA.

2.3.2 Preparation of DABCO Buffers for Hydrolysis

A stock solution of KCl (1.00 M) was prepared as before in Section 2.4.1. A stock solution of DABCO (1.00 M) was prepared by dissolving DABCO (56.09 g, 0.500 mol) in aqueous KCl (1.00 M, 500.0 mL). All stock solutions were filtered to remove dust. An appropriate volume (given in Table IV) of aqueous HCl (1.00 M) was added to the aqueous DABCO (1.00 M, 125 mL) to obtain the desired pH. These solutions were diluted to 250.0 mL with the prepared aqueous KCl solution (1.00 M) to maintain the ionic strength at 1.00 M (KCl).

Table IV. Volume of HCl (1 M) added to aqueous DABCO to obtain given pH

Buffer pH[a]	volume of 1.00 M HCl added (mL)
9.59	40.00
9.04	75.00
9.42	48.00

[a]Measured values

These buffer solutions were then diluted with aqueous KCl (1.00 M) to give the desired concentrations (see Table VI) of DABCO. These diluted buffers were used as the aqueous media for the determination of the observed pseudo first order hydrolysis rate constants for the hydrolysis of 1 in DABCO.

2.3.3 Preparation of Buffer Solutions (DABCO) for Measurement of Solvent Kinetic Isotope Effects

Buffer solutions in H_2O were prepared as previously described in section 2.4.2. Buffer solutions in D_2O were prepared in the following manner:

The stock solution of aqueous DCl was prepared by means of a reported method[29] using D_2O and benzoyl chloride. The 1.00 M solutions of DCl in D_2O were prepared by diluting the DCl solution with D_2O.

The buffer solutions of DABCO in D_2O were prepared in the same manner as the H_2O solutions, except that the aqueous DCl solution (1.00 M in D_2O) was used in place of the aqueous HCl solution (1.00 M). In this way, the buffer ratio (BH^+/B, where B = DABCO) for DABCO in D_2O was identical to that prepared with aqueous HCl and H_2O.

2.3.4 Amide and Buffer (DABCO) solutions for the Observation of Pseudo First Order Exchange Rate Constants

The amide solution was prepared by adding a solution of amide (40 mg in 2 mL DME) to an aqueous KCl solution (1.00 M) to attain a total volume of 100.0 mL and used in the syringe labelled 'amide solution' of Figure 22. A stock aqueous DABCO (1.00 M, μ = 1.00 M (KCl)) was prepared to the desired buffer ratio (BH^+/B = 2.13) by combining the recrystallised DABCO (2.80 g, 0.025 mol), aqueous HCl (8.00 mL, 1.00 M, 0.008 mol), and KCl (1.27 g, 0.017 mol) and dissolving in H_2O (25 ml). All of the stock solutions were passed through a sintered glass filter to remove any insoluble impurities. The resultant stock aqueous DABCO (0.500 M) was diluted with aqueous KCl (1.00 M) to obtain the buffer solutions of the following concentrations: 1.00 M (no dilution), 0.8, 0.6, 0.4, 0.2, 0.16, 0.12, 0.08, and 0.04 M. These diluted buffer solutions were used in the syringe labelled 'buffer solution' of Figure 22, so that when mixed with an equal volume of the amide solution with the use of the apparatus in Figure 22, gave final concentrations of aqueous DABCO equal to half that in the syringe.

2.4 Kinetics

2.4.1 Rate Constants for Hydrolysis of 1

The hydrolysis of **1** is associated with a decrease in the UV absorbance at 265 nm. Therefore, the observed pseudo first order hydrolysis rate constants (k_{obs}^{hyd}) for the hydrolysis of **1** in buffer solutions may be calculated from measured UV absorbance data as **1** hydrolyses to form *N*-*p*-nitrobenzoate and pyrrole. A buffer solution (3.0 mL, prepared as in Sections 2.3.1 and 2.3.2) was added to each cuvette and allowed to equilibrate to 25 °C for 30 minutes. An amide solution (20-50 μL, 4 mg/mL) was added to the equilibrated buffer solution and immediately and thoroughly mixed by inverting the

cuvette at least ten times. The cuvette was then replaced into the cell block of the spectrophotometer and the absorbance change was subsequently observed. Because the buffer (DABCO or TMA) also absorbs light in the UV region, the overall absorbance may vary as the concentration of buffer is varied. For this reason, the volume of added amide had to be reduced from 40 μL to 20 μL to maintain the total absorbance, as best as possible, near A = 2 when absorbance of the buffer was high. When the absorbance from the buffer was low, the volume of amide solution could be increased to 40 μL to obtain a larger absorbance change between the initial absorbance and the absorbance when hydrolysis of 1 was complete. The volume of the amide solution added does not affect the pseudo first order rate constant, therefore, the relative consumption of the buffer during the hydrolysis of 1 is negligible when compared to the consumption of 1. The absorbance change at 240 nm (TMA buffers), and at 278 nm (DABCO buffers) was observed for more than four half-lives for hydrolysis so that a maximum change in absorbance could be observed. All solutions were maintained at 25 °C.

$$A_t = \Delta A(1 - e^{-k_{obs}t}) + A_o \qquad \textbf{(10)}$$

$$\Delta A = A_o - A_\infty$$

A_o = initial absorbance (at $t = 0$)

A_∞ = absorbance at $t = \infty$

t = time

The raw absorbance versus time data was fit to equation 10 with the use of nonlinear least-squares regression analysis routine within the program Enzfit (v. 1.03) to obtain the observed pseudo first order rate hydrolysis constants, k_{obs}^{hyd}, for the reaction. The experimental error was estimated by using the range of three independent estimations of k_{obs}^{hyd} from UV absorbance versus time data.

Successive plots of absorbance versus wavelength data (Figure 23) were collected during the hydrolysis of **1** in the presence of TMA and DABCO between 250 and 320 nm. Isobestic points were observed on the successive plots for the hydrolysis of **1**. Isobestic points are observed at wavelengths where the extinction coefficients for the product are equal to those of the reactant, and the rate of product formation is equal to that of the reactant consumption. Therefore, any intermediates formed during the hydrolysis of **1** are short lived relative to the half-life for hydrolysis and do not accumulate on the time scale for hydrolysis.

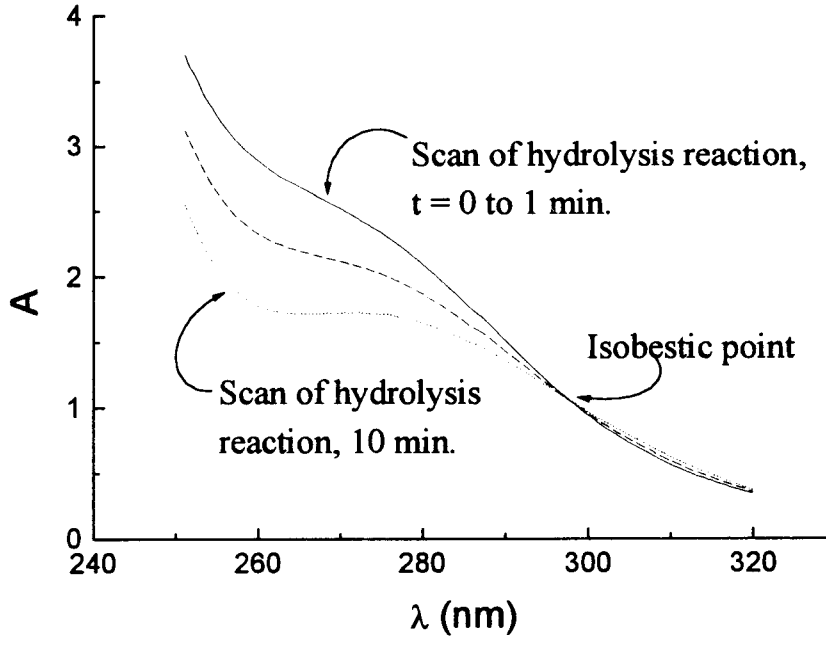

Figure 23. Successive plots of absorbance versus wavelength (λ, nm). First scan was collected starting at t = 0 s reaction time.

A product analysis by Menger and Donohue[4] showed that the molar extinction coefficients between 350 and 220 nm (observed at 5 nm intervals) for the hydrolysis products of **1** agreed within 10 percent of those obtained from a solution prepared from distilled pyrrole and *p*-nitrobenzoic acid.

2.4.2 Determination of hydrolysis rate constants in the presence of H_2O and D_2O and added DABCO

The observed pseudo first order hydrolysis rate constants for the hydrolysis of **1** in solutions containing D_2O or H_2O, and added DABCO were calculated from UV absorbance versus time data for the subsequent calculation of the SKIE. Buffer solutions were prepared as in Section 2.3.3 and used as the hydrolysis media for the determination of the SKIE. The hydrolyses were observed in the same manner as in Section 2.4.1 except that the absorbances of two buffer solutions (one H_2O and one D_2O solution corresponding to the same buffer ratio) were measured concurrently to minimise experimental error. The observed pseudo first order hydrolysis rate constant for the hydrolysis of **1** in each buffer solution was calculated independently from the concurrently collected absorbance versus time data by the use of nonlinear least-squares regression analysis as described in Section 2.4.1.

2.4.3 Determination of hydrolysis rate constants in the presence of OH^- and OD^- in the absence of buffer

The observed pseudo first order hydrolysis rate constants for the hydrolysis of **1** in solutions containing OH^- and OD^- in the absence of added buffer were calculated from observed UV absorbance (λ = 278 nm) versus time data.

Aqueous solutions of sodium hydroxide and sodium deuteroxide were prepared in the following manner.

A carbonate free solution of sodium hydroxide (approximately 14 M) was prepared by dissolving solid NaOH (36 g) into water (65 mL). A carbonate free solution of sodium

deuteroxide was prepared by adding sodium metal (20.7 g), in *small* portions, to D_2O (65 mL). (CAUTION: fire hazard!) The sodium hydroxide solution was assumed to be approximately 14 M, while an aliquot of the sodium deuteroxide solution was titrated with HCl (1 M) to determine its concentration (14.39 M in D_2O). These sodium hydroxide and deuteroxide solutions were diluted with H_2O and D_2O, respectively, to achieve a concentration of hydroxide and deuteroxide of approximately 1.0 M. The concentrations of hydroxide and deuteroxide ions were quantitatively determined by the use of titration with standard aqueous HCl (0.100 M). These hydroxide and deuteroxide solutions were further diluted with solutions of KCl in either H_2O and D_2O (1.00 M) to obtain solutions in which the pOL (L = H or D) ranged from 0.31 to 2.00 when mixed with an equal volume of KCl (1.00 M) containing **1** (4×10^{-4} M). The observed pseudo first order hydrolysis rate constants for hydrolysis of **1** in solutions of hydroxide and deuteroxide were calculated from the absorbance versus time data obtained with the use of a DURRUM 110 stopped-flow apparatus. The absorbance change was followed at λ = 278 nm, and the rate constants for hydrolysis were determined by the use of nonlinear least-squares regression analysis as previously described in Section 2.4.1.

2.4.4 Determination of Rate Constants for Exchange

All glassware used in contact with buffer or amide solutions was washed in concentrated nitric acid before its use to ensure the absence of impurities that might interfere with the mass spectrometric data. The glassware was then washed thoroughly with HPLC grade water, followed by washing with 95 percent ethanol (distilled at ambient pressure).

The amide and buffer solutions were placed into the syringes as described in Section 2.3.4. Initially, the buffer and amide solutions are passed through tubes that are immersed in the temperature controlled circulating water bath to equilibrate the

temperature of each solution to 25.0 ± 0.1 °C. The two solutions then mix at the 'three-way' connector and the hydrolysis of **1** proceeds as the combined solutions are passed through a reaction tube (length = 3 metres, total volume = 2.317 ± 0.023 mL). The combined solutions then elute into a collection vessel where the hydrolysis reaction is quenched by the use of the autoburrette and autotitrator apparatus that maintains the pH at 4. The retention time inside the reaction tube was always 1 half-life. The flow rate that was necessary to achieve a retention time of 1 half-life was determined from Equation 11.

$$\text{Required flow rate} = \frac{V}{t_{1/2}} \qquad \textbf{(11)}$$

where V = volume of reaction tube = 2.317 mL,
and $t_{1/2}$ = half-life for hydrolysis

The flow rates varied from 0.2 - 0.6 $mL \cdot s^{-1}$. The observed flow rate was measured by passing distilled water through the system and adjusting the flow rate until the calculated flow rate was equal to the average of three sequential measurements within the error range of the three measurements.

Any amide present in the reaction medium after the one half-life for hydrolysis was extracted with distilled methylene chloride (4 x 2 mL) within ½ h to minimise errors originating from any acid catalysed hydrolysis of **1**. The combined methylene chloride layers were washed with saturated sodium bicarbonate (2 x 4 mL each), water (2 mL), dried over $MgSO_4$, and passed through a glass wool filter to remove the solid $MgSO_4$. A lint-free tissue, small enough to be inserted into a melting point tube, was then deposited into the filtered methylene chloride solution containing the extracted amide. The solution was then allowed to evaporate to dryness at ambient temperature. The tissue was then inserted into the melting point tube and the ^{18}O content of the sample was determined by the use of mass spectrometry as described in Section 2.1.1. The absolute counts at $M^{\cdot+}$

and $M^{\cdot+} + 2$ were observed and the percentage ^{18}O content was calculated as the ratio of $\frac{M^{\cdot+}}{M^{\cdot+} \quad (M^{\cdot+} 2)} \times 100$. The observed pseudo first order exchange rate constant for the hydrolysis of **1** is calculated from the percentage *carbonyl*-^{18}O as in Equation 12.

$$k_{obs}^{ex} = \ln\frac{\left(\frac{A_i}{A_f}\right)}{t_{1/2}} \qquad \textbf{(12)}$$

where

A_i = Percentage *carbonyl*-^{18}O initial

A_f = Percentage *carbonyl*-^{18}O final

$t_{1/2}$ = half-life for hydrolysis

For the measurement of observed pesudo first order exchange rate constants for the hydrolysis of **1** with no added buffer, the amide (2 mg) was dissolved in an aqueous solution of KCl (10 mL, 1 M) containing a drop of HCl (1 M) to maintain low pH and prevent the hydrolysis of the amide. The pH was raised to the desired level with the use of the autoburette and autotitrator, maintained for a period of either 1 or 2 half-lives for hydrolysis, and then quenched by adding one drop of HCl (1 M). Any amide in the reaction medium was then extracted and prepared for analysis by the use of mass spectrometry as previously described. The calculated k_{ex}/k_{hyd} for the hydrolysis for 1 reaction half-live and 2 reaction half-lives agreed within the sum of half of each error range.

2.5 Determination of Structure

A single colourless needle-shaped crystal of **1** was formed from the slow evaporation of a solution containing isobutanol-hexane (1:1). The resulting crystal was mounted onto a glass fibre by means of epoxy adhesive. The structure of the solid crystal was determined by means of X-ray crystallography at the SFU X-ray crystallography laboratory.

Chapter 3

Data and Results

3.1 Rate Constants for the Hydroxide Ion- and Buffer-Promoted Hydrolysis of 1

The observed pseudo first order hydrolysis and exchange rate constants for the hydrolysis of 1 were calculated from UV absorbance versus time data. These data were collected by means described in the Experimental (Section 2.4.1). From these data, the function of hydroxide and buffer within the scheme for hydrolysis (Figure 14) may be proposed.

The hydrolysis of 1 is accompanied with a decrease in the UV absorbance in the region between 278 and 245 nm. Both the observed pseudo first order hydrolysis and exchange rate constants for the hydrolysis of 1 were calculated from the absorbance versus time data using Equation 13. A plot of the absorbance versus time data at pH = 9.41 in 0.50 M DABCO (Figure 24) shows the absorbance change at 278 nm versus time and the corresponding fit to Equation 10 from the Experimental Section. The χ^2_P (chi squared) for each fit to Equation 13 was the on the order of 10^{-8}.

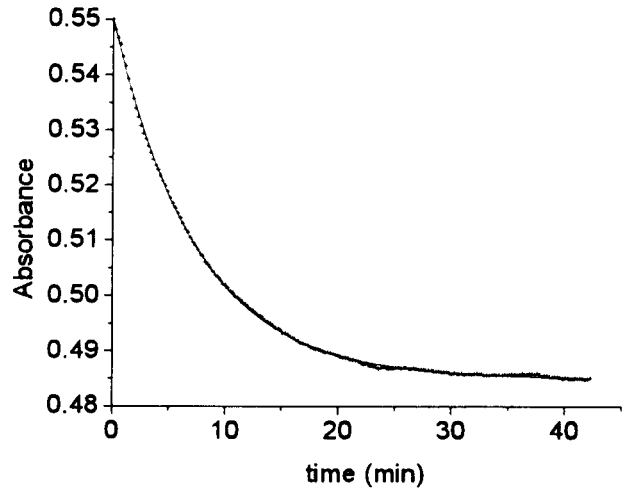

Figure 24. Absorbance change versus time during the hydrolysis of 1 in added DABCO. pH = 9.42, [DABCO] = 0.50 M, T = 25 °C, μ = 1.00 M (KCl). Best-fit line is calculated from Equation 10.

3.2 Dependence of the Hydrolysis Rate Constants on the Total Buffer Concentration

The observed pseudo first order rate constants, k_{obs}^{hyd}, for the hydroxide ion- and buffer-promoted hydrolysis of 1, given in Tables V and VI, show the dependence of k_{obs}^{hyd} on the concentration of added TMA and DABCO. Graphical representations of the dependence of k_{obs}^{hyd} on added TMA (pH = 10.55) and DABCO (pH = 9.59) are given in Figures 25 and 26, respectively. Similar plots may be constructed for each buffer and pH. Each k_{obs}^{hyd} from in Tables V and VI is the mean of three k_{obs}^{hyd} estimates. Each estimate was calculated from absorbance versus time data for the hydrolysis of 1 in three separate solutions of identical pH and buffer concentration. The experimental error for the average of the three k_{obs}^{hyd} estimates is estimated by using the range of the three estimates.

Table V. Observed pseudo first order hydrolysis rate constants for the hydrolysis of **1** in the presence of added TMA. T = 25 °C, μ = 1.00 M (KCl).

Buffer pH	[TMA] (M)	$(k_{obs}^{hyd} \pm \Delta k_{obs}^{hyd})^a$ x 10^3 (s^{-1})	Buffer pH	[TMA] (M)	$(k_{obs}^{hyd} \pm \Delta k_{obs}^{hyd})^a$ x 10^3 (s^{-1})
10.55	0.230	14.0 ± 0.3	9.41	0.230	1.30 ± 0.02
	0.184	13.9 ± 0.4		0.184	1.16 ± 0.02
	0.138	13.0 ± 0.1		0.138	1.10 ± 0.01
	0.092	12.50 ± 0.08		0.092	1.02 ± 0.004
	0.046	11.9 ± 0.1		0.046	0.910 ± 0.009
10.18	0.230	7.20 ± 0.03	9.11	0.230	0.60 ± 0.06
	0.184	6.9 ± 0.4		0.184	0.564 ± 0.006
	0.138	6.51 ± 0.05		0.138	0.528 ± 0.002
	0.092	6.17 ± 0.07		0.092	0.49 ± 0.01
	0.046	5.60 ± 0.05		0.046	0.41 ± 0.02
9.76	0.230	2.8 ± 0.2			
	0.184	2.71 ± 0.06			
	0.138	2.42 ± 0.06			
	0.092	2.32 ± 0.01			
	0.046	2.110 ± 0.009			

[a]Half the range (½R of three measurements) is used as the estimate of the experimental error.

Table VI. Observed pseudo first order hydrolysis rate constants for the hydrolysis of **1** in the presence of added DABCO. T = 25 °C, μ = 1.00 M (KCl).

Buffer pH	[DABCO] (M)	$(k_{obs}^{hyd} \pm \Delta k_{obs}^{hyd})^a$ x 10^4 (s^{-1})	Buffer pH	[DABCO] (M)	$(k_{obs}^{hyd} \pm \Delta k_{obs}^{hyd})^a$ x 10^4 (s^{-1})
9.59	0.50	28.8 ± 0.8	9.42	0.50	22.4 ± 0.3
	0.48	28.8 ± 0.7		0.48	22.3 ± 0.4
	0.44	27.6 ± 0.5		0.44	21.0 ± 0.4
	0.40	26.65 ± 0.08		0.40	20.3 ± 0.2
	0.36	25.5 ± 0.2		0.36	18.7 ± 0.2
	0.32	24.0 ± 0.3		0.32	18.60 ± 0.04
	0.28	23.0 ± 0.1		0.28	17.8 ± 0.2
	0.24	21.4 ± 0.5		0.24	16.47 ± 0.06
	0.20	20.2 ± 0.3		0.20	15.09 ± 0.07
	0.16	18.0 ± 0.8		0.16	14.4 ± 0.1
	0.12	17.5 ± 0.8		0.12	12.6 ± 0.1
	0.08	15.4 ± 0.1		0.08	11.3 ± 0.06
	0.04	13.6 ± 0.1		0.04	9.70 ± 0.03
	0.02	12.3 ± 0.2		0.02	8.95 ± 0.04

9.04	0.50	10.9 ± 0.1	0.20	7.35 ± 0.05
	0.48	10.5 ± 0.2	0.18	6.90 ± 0.06
	0.46	10.22 ± 0.07	0.16	6.64 ± 0.08
	0.44	9.89 ± 0.01	0.14	6.09 ± 0.08
	0.42	9.6 ± 0.1	0.12	5.8 ± 0.2
	0.40	9.81 ± 0.06	0.10	5.62 ± 0.05
	0.38	9.59 ± 0.06	0.08	5.17 ± 0.03
	0.36	9.3 ± 0.2	0.06	4.89 ± 0.04
	0.34	9.0 ± 0.1	0.04	4.450 ± 0.009
	0.30	8.52 ± 0.04	0.02	4.1 ± 0.2
	0.24	7.87 ± 0.07		

[a]Half the range (½R of three measurements) is used as the estimate of the experimental error.

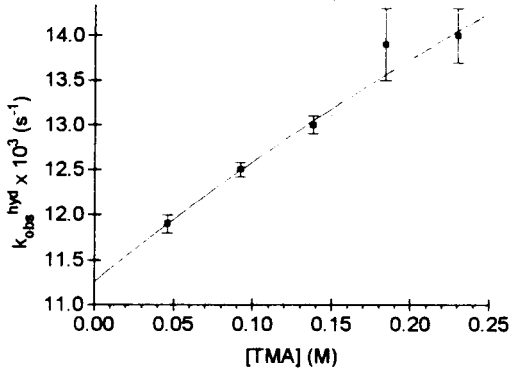

Figure 25. Observed pseudo first order hydrolysis rate constants for the hydrolysis of **1** in the presence of added TMA. pH = 10.55, T = 25 °C, μ = 1.00 M (KCl). Line is the calculated best-fit to Equation 13.

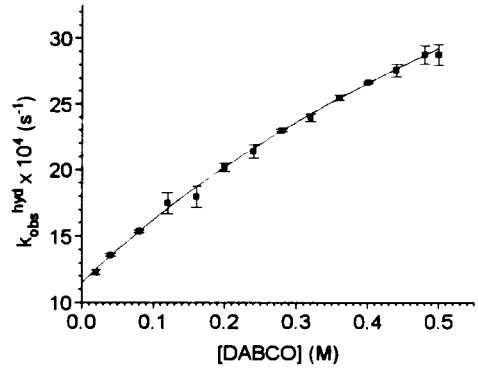

Figure 26. Observed pseudo first order hydrolysis rate constants for the hydrolysis of **1** in the presence of added DABCO. pH = 9.59, T = 25 °C, μ = 1.00 M (KCl). Line is the calculated best-fit to Equation 13.

These plotted data are concave-down curved within 1 range of the mean. This curvature is observed throughout all plots of k_{obs}^{hyd} versus TMA and DABCO concentrations. All of the curves were calculated according to the derived expression for hydrolysis rate constant in Equation 1, expressed as Equation 13 for the purpose of nonlinear regression. The four parameters, *A*, *B*, *C*, and *D*, of Equation 13 were first estimated by using the quasi-Newton routine for nonlinear least-squares regression

$$k_{obs}^{hyd} = \frac{A + B[\text{buffer}] + C[\text{buffer}]^2}{1 + D[\text{buffer}]} \qquad (13)$$

where $A = \frac{k_1 k_2}{k_{-1} + k_2}[OH^-]$, $\quad C = \frac{k_B k_{BP}}{k_{-1} + k_2}$,

$$B = \frac{k_1[OH^-]k_{BP} + k_2 k_B}{k_{-1} + k_2}, \quad D = \frac{k_{BH}K' + k_{BP}}{k_{-1} + k_2}.$$

within the program Systat (v. 5.01). The resulting estimates from the quasi-Newton method were used as the initial estimates for a second estimation of the parameters using the simplex routine for nonlinear least-squares regression, also within Systat. In most cases, the estimates from the quasi-Newton method agreed, within the standard error given by Systat, with the estimates from the simplex method. For each fit, χ^2_P was on the order of 10^{-10}. In some cases, however, the quasi-Newton and simplex routines would converge on local minima resulting in negative estimates of some parameters. A negative estimate implies a negative rate constant which is chemically meaningless according to the derived expression for the hydrolysis rate constant in Equation 1. For these cases, the parameters had to be constrained to be greater than zero during the nonlinear fits. Because Systat cannot constrain parameters, another program, MicroCal Origin (v. 3.0), was used so that the parameters could be constrained to be greater than zero. Estimates provided by Systat were used as the initial guesses for the estimation of the four parameters in MicroCal Origin, which led to chemically meaningful estimates of the parameters for Equation 13. MicroCal Origin was rarely successful at finding global minima without the initial guesses provided by Systat. The plots in Figures 25 and 26 show two such fits for hydrolysis in DABCO (pH = 9.59) and in TMA (pH = 10.55).

3.3 Function of Hydroxide Ion Concentration

The overall dependence of the hydrolysis rate on the hydroxide ion concentration, in the absence of buffer, was calculated by extrapolating the k_{obs}^{hyd} to zero buffer concentration to give the extrapolated rate constant, k^o_{calc}. At zero buffer concentration, k^0_{calc} ($= k^0_{hyd}$) depends only on the hydroxide ion concentration. According to the derived expression for the hydrolysis rate constant (Equation 1), when expressed as Equation 13, $\frac{k_1 k_2}{k_{-1} + k_2}[OH^-] = k^0_{hyd} = A$ at zero buffer concentration. However, there is no assumption within Equation 13 that $A = \frac{k_1 k_2}{k_{-1} + k_2}[OH^-]$ when Systat estimates the value of parameter A. These extrapolated, or estimated rate constants, can be plotted as $\log(k^o_{calc})$ versus pH. The resulting slope of the line is the overall order of hydroxide ion concentration in k^o_{calc} according to Equation 14.

By fitting k_{obs}^{hyd} and buffer data to Equation 13 as described in Section 3.2, parameter A becomes the estimate of k^0_{calc}. In Equation 14, n and k_{OH} are unknown. The value of n is the overall order of hydroxide ion concentration in k^0_{calc}.

Shown in Table VII are the estimated parameters, A and $\log(A)$, presented as k^o_{calc} and $\log(k^o_{calc})$, respectively, for each pH. The standard error calculated by Systat for parameter A is used as the estimate of the variance in k^o_{calc}.

Table VII. Calculated pseudo first order hydrolysis rate constants for the hydrolysis of 1 at zero buffer concentration (parameter A) versus pH. T = 25 °C, μ = 1.00 M (KCl).

pH	$(k^0_{calc} \pm \Delta k^0_{calc})$ x 10^4 (s^{-1})	$\log(k^0_{calc}) \pm \Delta\log(k^0_{calc})^a$ x 10^4 (s^{-1})
9.04	3.54 ± 0.06	-3.451 ± 0.007
9.11	3 ± 2	-3.5 ± 0.3
9.41	8.3 ± 0.2	-3.08 ± 0.01
9.42	8.20 ± 0.06	-3.086 ± 0.003
9.59	11.4 ± 0.3	-2.94 ± 0.01
9.76	19.3 ± 0.2	-2.714 ± 0.005
10.18	50 ± 10	-2.30 ± 0.09
10.55	112 ± 7	-1.95 ± 0.03

[a] $\Delta\log(k^0_{calc}) = \dfrac{\log(e)}{k^0_{calc}}\Delta k^0_{calc}$

To determine the order of hydroxide ion concentration in k^0_{calc} for the hydroxide ion-promoted hydrolysis of 1 in the absence of buffer, log(A) is plotted versus pH (Figure 27) according to Equation 14. These data were then fitted to the linear model in MicroCal Origin using the least-squares linear regression routine to obtain the slope of the line. The resulting slope is the overall order of hydroxide ion concentration in k^0_{calc} according to Equation 14, and the standard deviation of the slope is used as the estimate of the variance of the order of hydroxide ion concentration in k^o_{calc}. The calculated order is 1.03 ● 0.03. Depending on the relative magnitude of $k_3[OH^-] + k_2$ with respect to k_{-1}, the rate constant, k_{OH} may be either $\dfrac{k_1 k_2}{k_{-1} + k_2}$ or k_1, according to Equation 1. Because the overall order of hydroxide ion concentration is 1, the k_{OH} is a second-order rate constant. An estimate of k_{OH} may be made from each k^0_{calc} in Table VII. The average is an estimate of k_{OH} in this pH range which is 32 ● 1 $M^{-1}s^{-1}$. The error is estimated as the standard deviation of the calculated mean.

$$k^0_{calc} = k_{OH}[OH^-]^n \quad (14)$$

$$\log k^0_{calc} = \log k_{OH} + n\text{pH} - n14$$

where $k_{OH} = \dfrac{k_1 k_2}{k_{-1} + k_2}$ or k_1 of Equation 1

and n = order of hydroxide ion concentration.

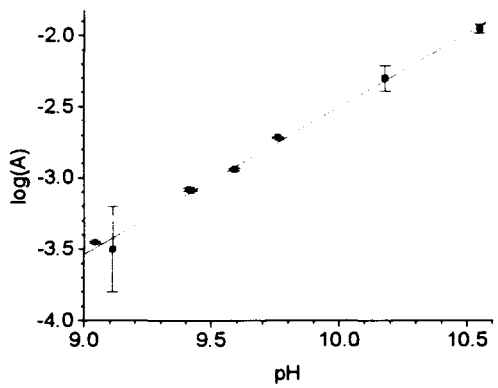

Figure 27. Calculated pseudo first order hydrolysis rate constants for the hydrolysis of **1** at zero buffer concentration (parameter A) versus pH. Slope = 1.03 ± 0.03; r = 0.997 T = 25 °C, μ = 1.00 M (KCl).

3.4 Solvent Deuterium Kinetic Isotope Effects (SKIE) in the Presence of Added DABCO

The SKIE cannot be calculated by means of Equation 13, but the effect may be qualitatively assessed. In Figure 28, the data for the aqueous base-promoted hydrolysis of **1** in H_2O and D_2O is plotted, both containing DABCO at identical buffer ratios. The overall slope for the hydrolysis in H_2O is larger than the overall slope for the same hydrolysis in D_2O, which corresponds to a SKIE greater than unity.

Table VIII. Observed pseudo first order hydrolysis rate constants for the hydrolysis of **1** in the presence of added DABCO in H_2O or D_2O. T = 25 °C, μ = 1.00 M (KCl), [B]/([B] + [BH^+]) = 1.5

[DABCO] (M)	$(k_{obs}^{hyd} \pm \Delta k_{obs}^{hyd})^a \times 10^4$ (s^{-1}) (in H_2O)	$(k_{obs}^{hyd} \pm \Delta k_{obs}^{hyd})^a \times 10^4$ (s^{-1}) (in D_2O)
0.5	8.94 ± 0.07	6.69 ± 0.03
0.4	8.3 ± 0.2	5.9 ± 0.2
0.3	7.4 ± 0.2	5.6 ± 0.1
0.2	5.97 ± 0.07	4.38 ± 0.06
0.1	4.6 ± 0.2	3.45 ± 0.05
0.04	3.5 ± 0.1	2.8 ± 0.2

[a]Half the range (½R of three trials) is used as an estimate of the experimental error.

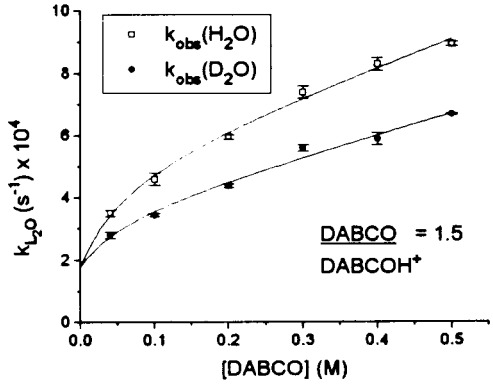

Figure 28. Observed pseudo first order hydrolysis rate constants for the hydrolysis of **1** in the presence of added DABCO in H_2O or D_2O. Buffer ratio = 1.5 (B/BH^+), T = 25 °C, μ = 1.00 M (KCl). Lines are best-fit lines to Equation 13.

3.5 The SKIE for the Hydroxide Ion-Promoted Hydrolysis of 1 (in the Absence of Buffer)

The observed SKIE for the lyoxide ion-promoted hydrolysis of **1** (lyoxide = hydroxide or deuteroxide) in the absence of buffer is the ratio of k^o_{obs} (extrapolated to molar hydroxide or deuteroxide). The k^o_{obs} in Tables IX and X were

calculated from the absorbance versus time data that are collected from the stopped-flow experiment as described in the Experimental Section. The error listed for each k^o_{obs} is the standard deviation calculated from eight k^o_{obs} that was calculated from eight independent observations of the absorbance versus time data for the hydrolysis of **1** at constant pOL (L = H or D). The SKIE is the ratio of $k^o_{obs}([OH^-] = 1)$ to $k^o_{obs}([OD^-] = 1)$ which are the antilogs$_{10}$ of the intercepts from Figure 29 for the hydroxide ion-promoted hydrolysis in H_2O or D_2O media, respectively. The calculated SKIE is 0.91 ± 0.04 (as k_{HOH}/k_{DOD}).

Table IX. Observed pseudo first order hydrolysis rate constants for the hydroxide ion-promoted hydrolysis of **1** in the absence of added buffer versus pOH. T = 25 °C, μ = 1.00 M (KCl).

pOH	$k^0_{obs} \pm \Delta k^0_{obs}$ [a] (s^{-1}) (H_2O)	$\log(k^0_{obs}) \pm \Delta\log(k^0_{obs})$ [b] (H_2O)
0.31	18.3 ± 0.5	1.26 ± 0.01
0.62	8.5 ± 0.3	0.93 ± 0.02
1.01	3.38 ± 0.06	0.529 ± 0.008
1.62	0.85 ± 0.02	-0.07 ± 0.01
2.01	0.325 ± 0.005	-0.488 ± 0.007
k_{1H_2O} ($M^{-1}s^{-1}$)	37 ± 1	

[a] Half the range (½R of three trials) is used as an estimate of the experimental error.

[b] $\Delta\log(k^0_{hyd}) = \dfrac{\log(e)}{k^0_{hyd}}\Delta k^0_{hyd}$

Table X. Observed pseudo first order hydrolysis rate constants for the deuteroxide ion-promoted hydrolysis of **1** in the absence of added buffer versus pOD. T = 25 °C, μ = 1.00 M (KCl).

pOD	$k^0_{obs} \pm \Delta k^0_{obs}$ [a] (s^{-1}) (D_2O)	$\log(k^0_{obs}) \pm \Delta\log(k^0_{obs})$ [b] (D_2O)
0.29	21.2 ± 0.2	1.326 ± 0.004
0.59	10.0 ± 0.5	1.00 ± 0.02
0.99	4.0 ± 0.2	0.60 ± 0.02
1.99	0.39 ± 0.02	-0.41 ± 0.02
k_{1D_2O} ($M^{-1}s^{-1}$)	40.7 ± 1	

[a] Half the range (½R of three trials) is used as an estimate of the experimental error.

[b] $\Delta\log(k^0_{hyd}) = \dfrac{\log(e)}{k^0_{hyd}}\Delta k^0_{hyd}$

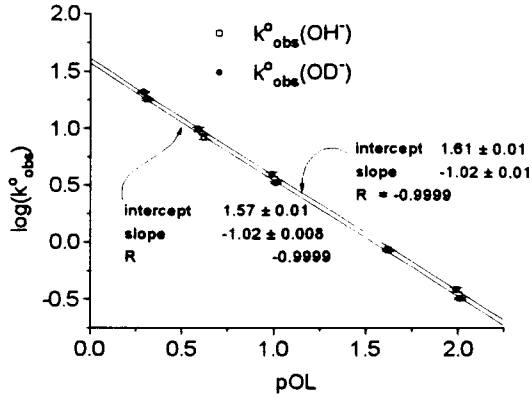

Figure 29. Observed pseudo first order hydrolysis rate constants for the lyoxide ion-promoted hydrolysis of **1** in the presence of hydroxide or deuteroxide. No added buffer. L = H or D.
T = 25 °C, μ = 1.00 M (KCl).

3.6 To⁻ Partitioning

The To⁻ partitioning is the ratio of the sum of the rate constants for To⁻ reversion to the amide starting material, to the sum of those for To⁻ breakdown to the products. Thus, the To⁻ partitioning is interpreted from the ratio of the observed pseudo first order exchange rate constant (k_{obs}^{ex}) and k_{obs}^{hyd} to give k_{ex}/k_{hyd}. The values of k_{ex}/k_{hyd} are listed in Table XI, along with the corresponding exchange and hydrolysis rate constants. The corresponding plot is in Figure 30. Each k_{obs}^{ex} is the mean of three estimates of the observed exchange rate constant that were calculated from the change in ^{18}O content as previously described in the Experimental (Section 2.4.4). The k_{obs}^{hyd} were calculated as previously described in Section 2.4.1.

Table XI. Observed pseudo first order exchange rate constants and the ratios of observed pseudo first order exchange rate constants to observed pseudo first order hydrolysis rate constants for the hydrolysis of **1** in the presence of added DABCO. pH = 9.48, T = 25 °C, μ = 1.00 M (KCl).

[DABCO] (M)	$(k_{obs}^{ex} \pm \Delta k_{obs}^{ex})^a \times 10^4$ ($M^{-1}s^{-1}$)	$(k_{obs}^{hyd} \pm \Delta k_{obs}^{hyd})^a \times 10^4$ ($M^{-1}s^{-1}$)	$k_{ex}/k_{hyd} \pm \Delta(k_{ex}/k_{hyd})^b$
0.5	5.1 ± 0.4	22.4 ± 0.1	0.23 ± 0.02
0.4	4.5 ± 0.3	21.3 ± 0.4	0.21 ± 0.02
0.3	4.5 ± 0.6	19.1 ± 0.6	0.23 ± 0.03
0.2	3.7 ± 0.2	16.0 ± 0.6	0.23 ± 0.01
0.1	2.6 ± 0.2	12.7 ± 0.3	0.20 ± 0.01
0.08	2.0 ± 0.3	12.1 ± 0.8	0.17 ± 0.03
0.06	1.8 ± 0.4	11.6 ± 0.3	0.15 ± 0.03
0.04	1.8 ± 0.3	10.7 ± 0.2	0.16 ± 0.03
0.02	1.6 ± 0.3	10.4 ± 0.4	0.15 ± 0.03
0.00	0.5 ± 0.2	9.2 ± 0.5	0.06 ± 0.03

[a]Half the range (½R of three measurements) is used as an estimate of the experimental error.

[b] $$\Delta\left(\frac{k_{ex}}{k_{hyd}}\right) = \sqrt{\left(\frac{\Delta k_{obs}^{ex}}{k_{obs}^{hyd}}\right)^2 + \left(\frac{k_{obs}^{ex}}{-\left(k_{obs}^{hyd}\right)^2}\right)^2 \left(\Delta k_{obs}^{hyd}\right)^2}$$

For the purpose of nonlinear least-squares regression analysis, the derived

$$\frac{k_{ex}}{k_{hyd}} = \frac{K_1 + K_2[B]_T}{1 + K_3[B]_T} \qquad (15)$$

where

$$K_1 = \frac{k_{-1}}{2k_2} \qquad K_2 = \frac{k_{BH}}{2k_2}(1-\chi_B) \qquad K_3 = \frac{k_{BP}}{k_2}\chi_B$$

expression for k_{ex}/k_{hyd} (Equation 3) may be expressed as in Equation 15. Equation 15 requires only three parameters to be estimated by Systat, whereas Equation 3 would

require four parameters. The parameters, K_1, K_2, and K_3, listed in Table XII were estimated by using nonlinear least-squares regression, as previously described in Section 3.2. The derived expression for k_{ex}/k_{hyd} (Equation 3) may also be expressed as Equation 16. This form of the derived expression for k_{ex}/k_{hyd} also requires only three parameters (K_4, K_5, and K_6) to be estimated by Systat, also listed in Table XII.

$$\frac{k_{ex}}{k_{hyd}} = \frac{K_4 + K_5[B]_T}{K_6 + [B]_T} \qquad (16)$$

where

$$K_4 = \frac{k_{-1}}{2k_{BP}\chi_B} \qquad K_5 = \frac{k_{BH}}{2k_{BP}}\left(\frac{1-\chi_B}{\chi_B}\right) \qquad K_6 = \frac{k_2}{k_{BP}\chi_B}$$

An estimate of k_B and a second estimate of k_{BP}/k_2 is possible by using the estimates of k_{-1}/k_2 and k_{BH}/k_{BP} from K_1 and K_5 in Equations 15 and 16, and the value of k_1 obtained from Section 3.5. The estimates of k_B and k_{BP}/k_2 are obtained by the use of nonlinear least-squares regression analysis as previously described, using Equation 17 which is derived from Equation 1. Equation 17 is plotted in Figure 31 at pH 9.04 by using the estimates k_B and k_{BP}/k_2, and the value for k_1. The fitted line of Equation 17 traverses half of the points at pH 9.04 within one range.

$$k_{hyd}^{obs} = \frac{(37.15[OH^-] + k_B[B])(1 + \frac{k_{BP}}{k_2}[B])}{(1.1 + \frac{k_{BP}}{k_2}([B] + [BH^+])} \qquad (17)$$

Table XII. Rate constants and ratios of rate constants calculated from experimental data using nonlinear least-squares regression. $\chi_B = 0.68$

Parameter	Definitions of parameters	Value ± error[a]
K_1	$\frac{k_{-1}}{2k_2}$	0.05 ± 0.02
K_2	$\frac{k_{BH}}{2k_2}(1-\chi_B)$ (M^{-1})	8 ± 3
K_3	$\frac{k_{BP}}{k_2}$ (M^{-1})	35 ± 16
K_4	$\frac{k_{-1}}{2k_{BP}\chi_B}$ (M)	0.0013 ± 0.0009
K_5	$\frac{k_{BH}}{2k_{BP}}\left(\frac{1-\chi_B}{\chi_B}\right)$	0.235 ± 0.014
K_6	$\frac{k_2}{k_{BP}\chi_B}$ (M)	0.028 ± 0.011
k_B ($M^{-1}s^{-1}$)		0.0070 ± 0.0002
K_3 (M^{-1})		3.0 ± 0.4

[a]Standard error calculated from Systat.

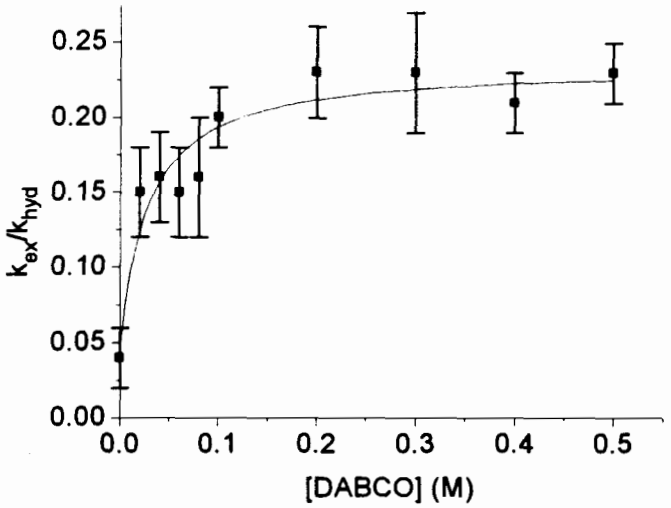

Figure 30. k_{ex}/k_{hyd} versus total concentration of added DABCO. Line is calculated best-fit to Equation 15. T = 25 °C, μ = 1.00 M (KCl).

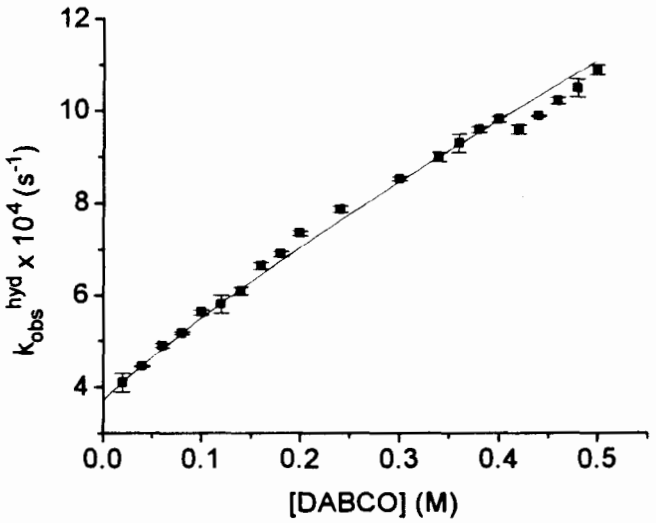

Figure 31. Observed pseudo first order hydrolysis rate constants for the hydrolysis of **1** in the presence of added DABCO. pH = 9.04, T = 25 °C, μ = 1.00 M (KCl). Line is calculated from Equation 17.

3.7 Structure of 1

The amide C–N bond distance and torsional angles within the amide unit of **1** are obtained from X-ray crystallography for the comparison with the similar amide, **2**. Bond distances within the amide unit are listed in Table XIII, and torsional angles are in Table XV. The crystal structure is shown in Figure 32. The crystal lattice of **1** is monoclinic with a space group $P2_1/c$; the unit cell dimensions are a = 6.027(3), b = 21.832(5), and c = 7.580(3) Å, and β = 98.63(3) °. R = 0.176.

Table XIII. Selected bond distances for **1**.

Bond	Distance (Å) ± error[a]
O(8)–C(8)	1.216 ± 0.003
N(8)–C(9)	1.398 ± 0.003
N(8)–C(12)	1.395 ± 0.003
N(8)–C(8)	1.386 ± 0.003
C(8)–C(7)	1.491 ± 0.003

[a]Error is that given by the computer program CRYSTALS.

Table XIV. Selected torsional angles for **1**.

Torsional angle	angle ± error[a]
C(9)–N(8)–C(8)–O(8)	-172.7 ± 0.3
C(12)–N(8)–C(8)–O(8)	6.4 ± 0.1
C(9)–N(8)–C(8)–C(7)	8.5 ± 0.1
C(12)–N(8)–C(8)–C(7)	-172.5 ± 0.2

[a]Error is that given by the computer program CRYSTALS.

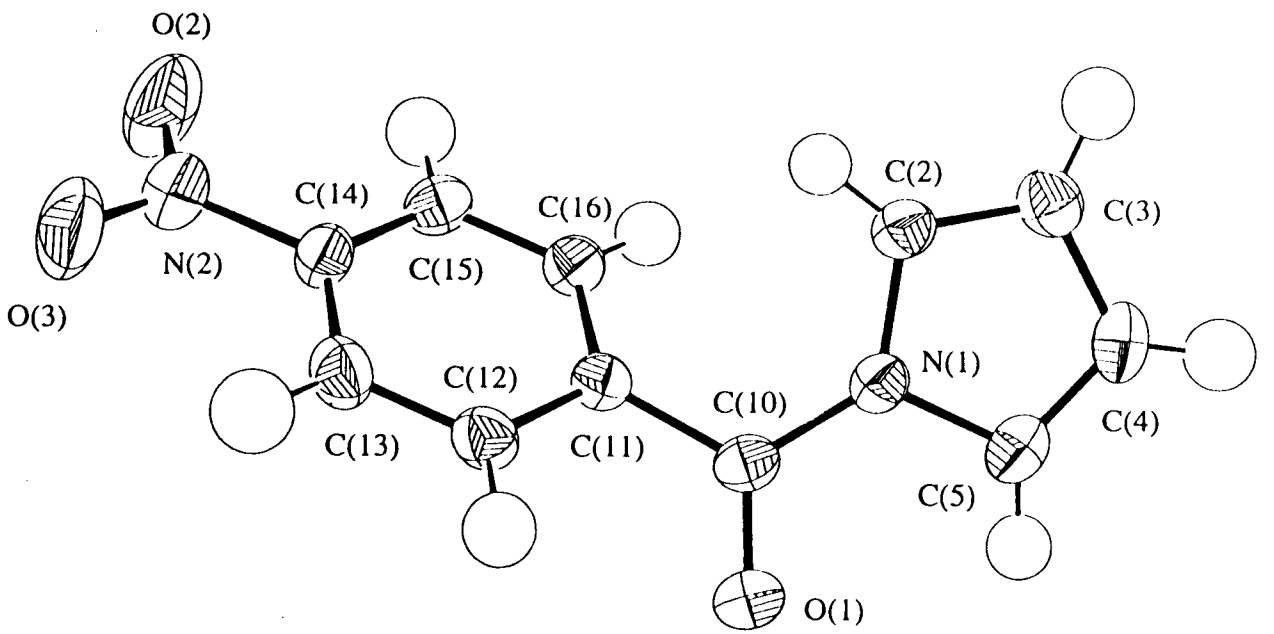

Figure 32. Crystal structure of **1**; Ortep drawing of the 50% enclosure ellipsoids are shown.

Chapter 4

Kinetics and Mechanism for the Aqueous Base- and Buffer-Promoted Hydrolysis of *N-p*-Nitrobenzoylpyrrole

4.1 Use of the Derived Expression for k_{obs}^{hyd} in the Analysis of k_{obs}^{hyd} Versus Added Buffer

All of the kinetic data for the aqueous base- and buffer-promoted hydrolysis of the amide, **1**, were interpreted according to the derived expressions for k_{obs}^{hyd} (Equation 1) and k_{obs}^{ex} (Equation 2). The derived expression for k_{obs}^{hyd} is not a linear function of the buffer concentration. However, if the experimental data were randomly distributed about a straight line, the approximation that $k_2 + k_{BP}[B] + k_3[OH^-] >> k_{-1} + k_{BH}[BH^+]$ may be applied to Equation 1 to render a linear expression. For k_{obs}^{hyd}, the linear approximation implies that To^- formation is completely rate limiting.

A linear function does not traverse each k_{obs}^{hyd} within one range of the observed data in Figure 33. Furthermore, if a linear function could traverse each k_{obs}^{hyd} within two or three ranges, the resulting residual would not be randomly distributed about the line y = 0 (circles in Figure 34). Consequently, a linear approximation of Equation 1 does not estimate all of the experimental data within one range. The derived expression for the aqueous base- and buffer-promoted hydrolysis (Equation 1), when written as Equation 13, was successfully fit to the experimental data. The resulting fit traverses each k_{obs}^{hyd} within one range of the observed data, and produces a residual that is randomly distributed about

the line y = 0 in Figure 34. Consequently, the fit to Equation 13 predicts the k_{obs}^{hyd} more accurately than does the fit to a linear approximation.

The value of the parameter '*A*' in Equation 13 is assumed equal to $\frac{k_1 k_2}{k_{-1}+k_2}[OH^-]$ rather than $k_1[OH^-]$ in the pH range 9–10.5. This assumption applies only to the interpretation of the parameter '*A*', and has no effect on the numerical estimation by means of the nonlinear least-squares regression.

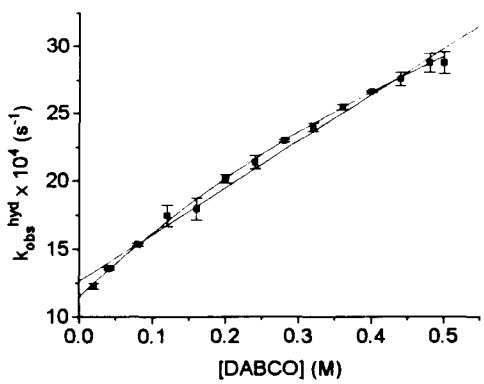

Figure 33. Observed pseudo first order hydrolysis rate constants, best-fit curve calculated by nonlinear least-squares regression, and a linear approximation. The linear approximation does not traverse each point within one range. pH = 9.59.

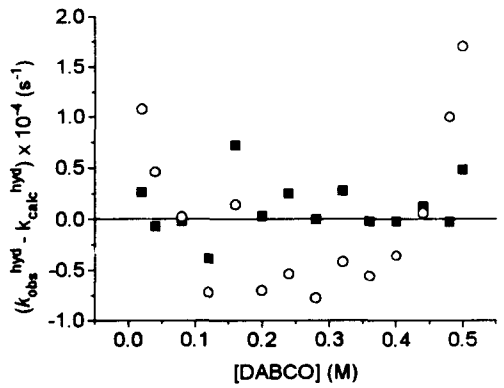

Figure 34. Residuals as $k_{calc}^{hyd} - k_{obs}^{hyd}$ from the hydrolysis at pH = 9.59 with added DABCO. Residual from the linear approximation has a systematic distribution about $y = 0$. ■ = residual from nonlinear fit; ○ = residual from linear fit.

While the calculated estimates of each k_{obs}^{hyd} from Equation 13 agree within one range of the observed data, it cannot accurately predict the k_{obs}^{hyd} for buffer concentrations greater than those studied. According to Equation 13, the experimental data for k_{obs}^{hyd} should approach the asymptote given by k_{obs}^{hyd} = B/D + (C/D)[B] at high buffer concentrations. However, the experimental data do not sufficiently describe this asymptote in the buffer concentration range studied.

4.2 Mechanistic Function of Hydroxide Ion

The proposed scheme for the aqueous base-promoted hydrolysis of **1** suggests that hydroxide ions should promote To$^-$ formation at all pH levels, and sometimes catalyse To$^-$ breakdown as well. The evidence from the order of hydroxide ion concentration provides the information needed to postulate the transition states for both To$^-$ formation and breakdown.

For the aqueous base-promoted hydrolysis of **1**, within the pH range 9–10.5, the overall observed order of the hydroxide ion concentration is 1. This observed order agrees with only two possibilities for k_{obs}^{hyd}, within the proposed scheme in Figure 14, which becomes $k_{hyd}^{0} = \dfrac{k_1[OH^-](k_2+k_3[OH^-])}{k_{-1}+k_2+k_3[OH^-]}$ at zero buffer concentration. According to this equation for k^0_{hyd}, the overall order is 1 if either $k_3[OH^-] << k_2$ to give k^0_{hyd} = Equation 18, or $k_3[OH^-] + k_2 >> k_{-1}$ to give $k^0_{hyd} = k_1[OH^-]$. In either case, the hydroxide ion is associated with aqueous base-promoted To$^-$ formation. The evidence from the aqueous base-promoted hydrolysis of **2** suggests that $k_3[OH^-]$ is negligible[21] with respect to k_2 in this pH range, and gives the overall k^0_{hyd} as Equation 18.

$$k_{hyd}^{0} = \frac{k_1 k_2[OH^-]}{k_{-1}+k_2} \qquad \textbf{(18)}$$

The order of hydroxide ion concentration for To$^-$ formation requires that the associated transition state contains the stoichiometric equivalent of one hydroxide ion and one amide molecule. Therefore, the transition state for To$^-$ formation must be monoanionic overall and the proposed transition state is shown in Figure 35. The evidence from the aqueous base-promoted hydrolysis of **2** suggests that To$^-$ breakdown is unimolecular in the pH range 9–10.5, also requiring a monoanionic transition state composed of only the To$^-$, which is given in Figure 36a.

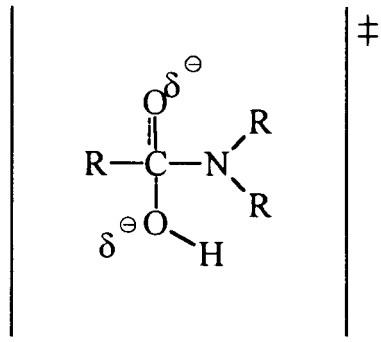

Figure 35. Proposed transition state for the aqueous base-promoted To$^-$ formation of **1**.

When the aqueous base-promoted hydrolysis of **1** is studied at higher pH ranges (pH = 12–14), the observed order of hydroxide ion concentration is also indistinguishable from unity within 2 sample standard deviations of the mean observed order. Because the observed order is unity, k^0_{obs} is consistent with either k^0_{hyd} = Equation 18 or $k_1[OH^-]$. From the observation that hydroxide ion catalyses To$^-$ breakdown of **2** in this pH range, we propose that hydroxide ion also catalyses To$^-$ breakdown (of **1**) so that $k_3[OH^-] + k_2 >> k_{-1}$ and thus $k^0_{hyd} = k_1[OH^-]$. In this pH range, the dependence of k^{hyd}_{obs} on hydroxide ion concentration requires that hydroxide ion be incorporated into the transition state for To$^-$ formation to form the same transition state found in lower pH ranges (Figure 40).

In this pH range (12–14), the evidence from **2** suggests that the hydroxide ion is incorporated in the mechanistic scheme during To$^-$ breakdown. Another amide, *N*-toluoyltetrafluoropyrrolidine, also exhibits hydroxide ion catalysis of To$^-$ breakdown.[21] The transition state in Figure 36b was proposed for To$^-$ breakdown of *N*-toluoyl tetrafluoropyrrolidine. For a lack of further direct evidence concerning the hydroxide ion catalysis of To$^-$ breakdown (of **1**), we propose that the transition state (Figure 36b) for this To$^-$ breakdown should not be any different from that proposed for *N*-toluoyl tetrafluoropyrrolidine.

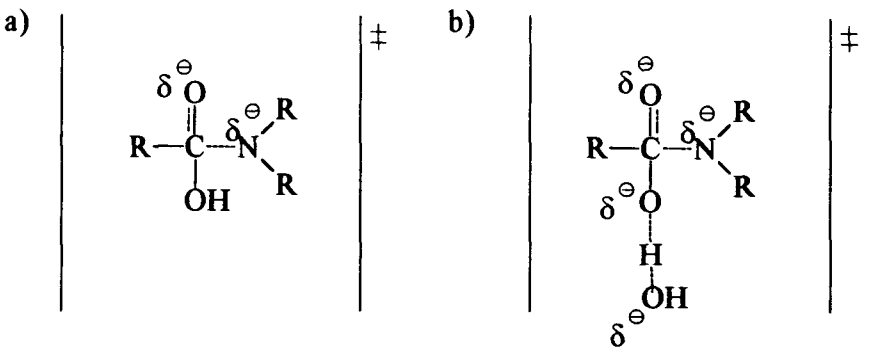

Figure 36. Transition states for (a) unimolecular and (b) hydroxide ion promotion of To$^-$ breakdown.

More noteworthy evidence for k_3 comes from two estimates of k_{OH}. Where hydroxide ions do not catalyse To$^-$ breakdown, rate constant k_{OH} is second-order overall and given as $\frac{k_1k_2}{k_{-1}+k_2}$. Where hydroxide ions do catalyse To$^-$ breakdown, k_{OH} is k_1, a first-order rate constant. When k_{OH} is calculated at each pH range (9–10.5 and 12–14), two estimates for k_{OH} are obtained and are distinguishable within two standard errors. At low pH, $k_{OH} = (32 \pm 1)\ M^{-1}s^{-1}$ (average k_{OH} calculated from each k^0_{calc} at pH 9–10.5), whereas at high pH the $k_{OH} = (37 \pm 1)\ M^{-1}s^{-1}$. The only way both calculated values of k_{OH} can be valid in their respective pH ranges is if at low pH ranges $k_{OH} = \frac{k_1k_2}{k_{-1}+k_2}$ and that at high pH ranges $k_{OH} = k_1$.

An estimate of k_{-1}/k_2 is possible from this hydrolysis data, and can be compared with the estimate obtained from k_{ex}/k_{hyd} at zero buffer concentration. From the k^{hyd}_{obs} data, the k_{-1}/k_2 can be estimated to be 0.16, whereas from the k_{ex}/k_{hyd} data, the k_{-1}/k_2 was observed to be 0.1 ■ 0.04. That the magnitudes of both estimates are similar suggests that the assumptions that lead to each estimate for k_{OH} are valid, and therefore To$^-$ breakdown is catalysed by hydroxide ion at high pH ranges.

4.3 Buffer in Formation of Tetrahedral Intermediate, To$^-$

Where buffer catalysis or promotion is observed, its effect must be on the rate limiting step. The evidence that To$^-$ partitioning always favours product formation from

To^- ($k_{ex}/k_{hyd} < 0.5$), requires that To^- formation is formally rate limiting at all pH levels and buffer concentrations studied. Because the buffer promotes the hydrolysis of **1** (Figures 25 and 26), it must enhance the rate of To^- formation, which is the rate limiting step.

Further evidence for the buffer-promoted To^- formation comes from the observed changes in To^- partitioning (see Figure 30) as the buffer is added. The k_{ex}/k_{hyd} ratio increases, so that To^- partitioning increasingly favours To^- reversion to amide as the buffer concentration is increased. According to Equation 3, the k_{ex}/k_{hyd} ratio can only increase if $k_{BH}[BH^+] > 0$, and the condition that $k_{BH} = 0$ could only lead to either an unchanging or a decreasing k_{ex}/k_{hyd} as the buffer concentration is increased. The principle of microscopic reversibility requires that, if $k_B > 0$, then $k_{BH} > 0$ also. The observed To^- partitioning is clearly inconsistent with buffer-promoted To^- breakdown only, but is consistent with buffer-promoted To^- formation.

4.4 Buffer in Breakdown of Tetrahedral Intermediate, To^-

The necessary information that establishes buffer-promoted To^- breakdown comes from the observed changes in To^- partitioning as the buffer concentration varies (at a constant buffer ratio). According to Equation 3 and with the knowledge that $k_B > 0$, if $k_{BP} > 0$ the change in To^- partitioning should cease to be dependent on the buffer concentration as the total buffer concentration becomes high and $k_{BP}[B] >> k_2$, $k_{BH}[BH] >> k_{-1}$, and $\frac{k_{ex}}{k_{hyd}} = \frac{k_{BH}[BH]}{k_{BP}[B]}$ at a constant buffer ratio (which requires constant pH). If, however, $k_{BP} = 0$, the change in To^- partitioning would be linearly dependent on the total buffer concentration. At high buffer concentrations, the slope of k_{ex}/k_{hyd} versus buffer concentration in Figure 30 cannot be distinguished from zero, and can only be consistent with $k_{BP} > 0$, i.e. buffer-promoted To^- breakdown.

4.5 Transition States for Buffer-Promoted Breakdown and Formation of Tetrahedral Intermediate, To⁻

Again, because To⁻ formation is formally rate limiting, k_{obs}^{hyd} versus buffer data do not reveal much about buffer-promoted To⁻ breakdown. However, the conclusion that hydroxide ion catalyses To⁻ breakdown suggests that the basic buffer species catalyses the breakdown by way of general-base catalysis. In the proposed transition state for the hydroxide ion-catalysed To⁻ breakdown, the remaining To⁻ hydroxyl proton is removed concurrently with C–N cleavage to form, initially, carboxylate, pyrrole anion, and a water molecule. A subsequent proton transfer from the solvent to the pyrrole anion regenerates the hydroxide ion, which meets the requirement for catalysis. The same proton on To⁻ is removable by the basic buffer species, and this process forms the postulated transition state that incorporates To⁻ and the basic buffer species in Figure 37.

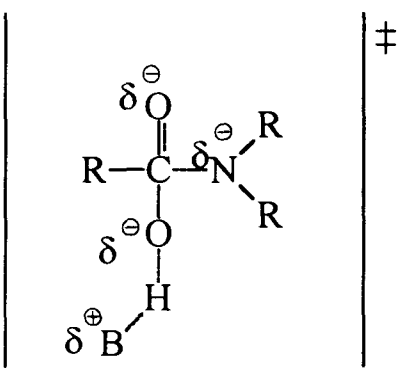

Figure 37. Proposed transition state for buffer-promoted To⁻ breakdown.

The mechanistic function of the buffer in To⁻ formation is interpreted from the dependence of k_{obs}^{hyd} versus the fraction of the basic buffer species, χ_B for TMA. The overall slope of each plot in Figure 38 increases as the pH increases, and approaches zero as the χ_B approaches zero. The observation that there is little catalysis by the buffer when the χ_B is small indicates that the acidic buffer species is not important during To⁻ formation, which is the rate limiting step at low buffer concentrations. Conversely, as the χ_B increases, promotion by the buffer becomes evident from the positive slopes in

Figure 38. These results are all consistent with the basic buffer promotion of To^- formation. A transition state for To^- formation is in Figure 39. A similar trend was observed for the DABCO promoted hydrolysis of **1**, although a narrower χ_B range was studied using this buffer.

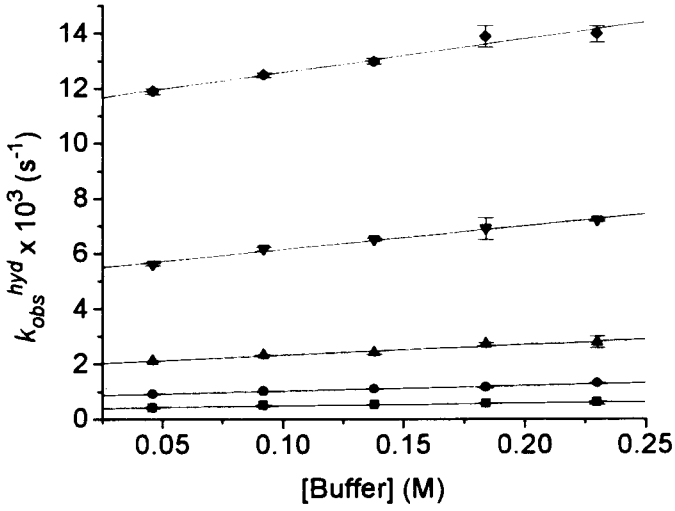

Figure 38. The dependence of k_{obs}^{hyd} on total buffer concentration for each pH. ■ pH = 9.11; ● pH = 9.41; ▲ pH = 9.76; ▼ pH = 10.18; ◆ pH = 10.55.

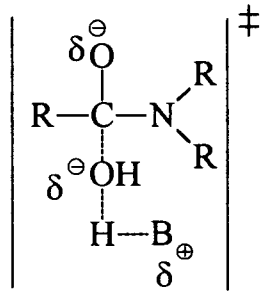

Figure 39. Proposed transition state for buffer-promoted To^- formation.

4.6 The Estimation of the Solvent Kinetic Isotope Effect

A reliable estimate of k_{HOH}/k_{DOD} for the SKIE on k^0_{obs} (in the pH range 12–14) is contingent upon the assumption that $k_2 + k_3[OH^-] >> k_{-1}$ is valid, so that $k^0_{hyd} \rightarrow k_1[OH^-]$. Although To$^-$ partitioning was not observed in this pH range, the aqueous base-promoted hydrolysis rate constants are consistent with $k_{OH} = k_1[OH^-]$ in this pH range. The estimated SKIE was evaluated by means of Equation 7 and using the fractionation factors for the To$^-$ formation given in Figure 40. The observed SKIE for the aqueous base-promoted To$^-$ formation is 0.91 ± 0.04 and agrees with the estimated SKIE within the given error (0.91 for $\alpha = 0.6$; 0.93 for $\alpha = 0.7$, where α is the position of the transition state along the reaction coordinate). Thus, the proposed transition state for the aqueous base-promoted To$^-$ formation from **1** is supported by the SKIE.

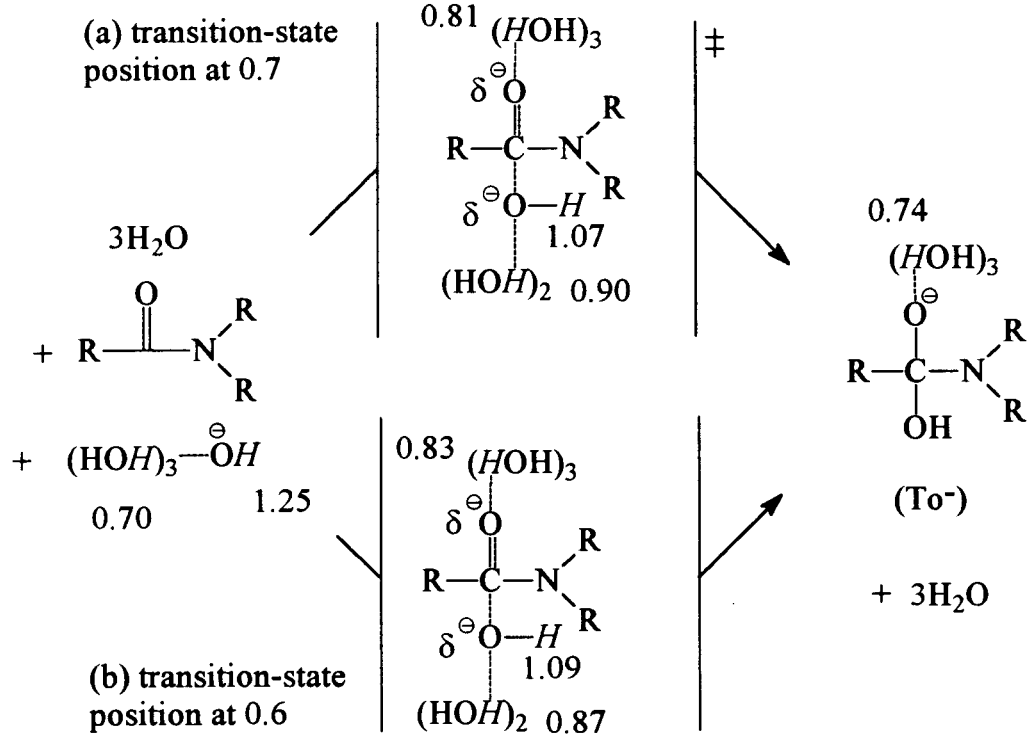

Figure 40. Fractionation factors, associated with italic *H*, for the estimation of the SKIE for aqueous base-promoted To$^-$ formation. Hydrogens to which the fractionation factors apply are indicated by *H*. (a) Calculated Φ for transition-state position at 0.7. (b) Calculated Φ for transition-state position at 0.6. Φ Calculated by means of Equation 9.

The SKIE on k_B is more difficult to accurately determine because as buffer is added, To$^-$ formation becomes less rate limiting. Nevertheless, To$^-$ formation remains predominantly rate limiting for all conditions where the SKIE was observed in the presence of added buffer, so that most of the observed SKIE may be attributed to To$^-$ formation. At the pH where the observation of SKIE on k_B was attempted, the addition of the buffer resulted in To$^-$ partitioning of $k_{ex}/k_{hyd} < 0.2$.

A normal SKIE, observed as the divergent slopes in Figure 28, is consistent with the transition state for buffer-promoted To$^-$ formation in Figure 39. The estimated SKIE for k_B (as k_{HOH}/k_{DOD}) is 3.5, calculated using the fractionation factors in Figure 41. Large normal SKIEs are usually expected when a proton is transferred at the rate limiting step, as proposed in Figure 41. Because the fractionation factor for the proton 'in flight' cannot be adequately estimated in Figure 41 the magnitude of the observed SKIE on k_B cannot be estimated accurately. Furthermore, an SKIE on To$^-$ breakdown (k_{BP}) also contributes to the total observed SKIE. Although this contribution to the total SKIE will be small (k_B is predominantly rate limiting), it remains unknown.

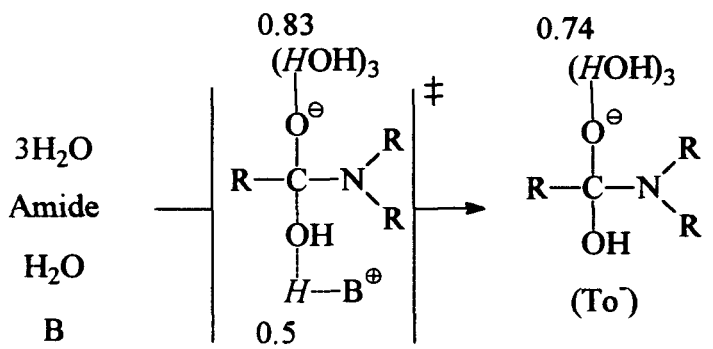

Figure 41. Φ, associated with italic *H*, for buffer-promoted To$^-$ formation. The Φ for the proton 'in flight' takes an average value of 0.5. Other Φ at the transition state are calculated by using Equation 9.

Chapter 5

Perspectives on Amide Resonance

5.1 The Crystal Structure of 1

The crystal structure of **1** reveals that the planar conformation is preferred in the solid state. Upon comparison with other crystalline amides, **1** possesses negligible tilt, and only minimal twist. The pyrimidalisations at both C(1) and N(3) are essentially nonexistent; all other amides listed in Table XV have at least a minor pyrimidalisation at either C(1) or N(3). The observed C(1)–N(3) bond length is longer in **1** (1.386 Å) than in formamide (1.32 Å), but the observed C(1)–O(1) bond length is unchanged relative to that of formamide (1.22 Å). The only significant structural difference between **1** and **2** is the C(1)–N(3) bond length which is slightly longer in **2** (1.41 Å).

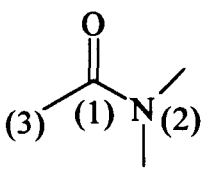

Figure 42. Numbering system for the amide.

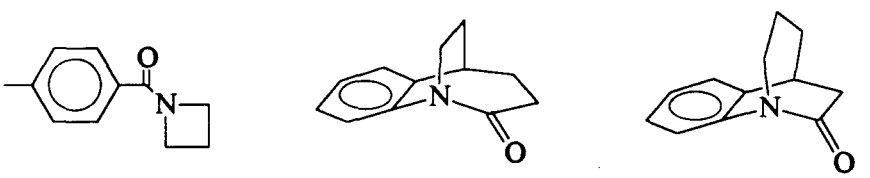

4 5 5a

Figure 43. Distorted amides from reference 11

Table XV. Second-order hydrolysis rate constants for hydrolysis and corresponding distortion parameters of various amides.

Amide	r(C–O) (Å)	r(C–N) (Å)	k_1 ($M^{-1}s^{-1}$)	χ_C [a] (°)	χ_N [a] (°)	twist[b] (°)	tilt[b] (°)
4	1.236(7)[c]	1.339(7)[c]	4.01(5) x 10^{-5} [d]	0.7[c]	32.5[c]	3.3[c]	7.5[c]
2	1.211(5)[c]	1.409(5)[c]	1.81(3)[e]	0[c]	10.1[c]	7.9[c]	2.6[c]
5	1.216(2)[d]	1.401(2)[d]	60(3)[d]	9[d]	57[d]	30.7[d]	15.2[d]
1	1.216(3)	1.386(3)	37(1)	1.1	1.0	7.4	0.3
5a	1.225(7)	1.413(10)	17.2(1.7)[d]	11[d]	53[d]	33[d]	16[d]
	1.233(10)[d,f]	1.419(11)[d,f]					

[a] Dunitz parameters,[30] where χ_C and χ_N relate to the amount of pyramidalisation at C(1) and N(3), respectively.
[b] Defined in reference 31.
[c] Reference 11.
[d] Reference 31.
[e] Reference 21.
[f] Two crystallographically independent molecules in unit cell were reported in reference 31.

Organic chemists would like a simple qualitative model that rationalises the reactivity of all amides. For many years, the resonance theory has served to explain the reactivity of amides and other organic molecules. However, support for amide resonance may be faltering. Wiberg and Laidig[9] observed that the C(1)–O(1) bond distance is only scarcely affected by rotation about the C(1)–N(2) bond, contrary to that expected from the resonance theory, as conventionally invoked for amides. Also contrary to the resonance theory, the calculated electron population[9] at N(2) in the planar amide (Figure 8) is greater than that in the orthogonal rotamer . As an alternative to the resonance theory, Bennet et. al.[11] proposed that the rate constant, k_1, is related to the magnitude of N pyrimidalisation (χ_N) and C(1)–N(2) bond lengthening for distorted amides. However, the magnitude of the χ_N in **1** is, if anything, less than that in **2**, and the C(1)–N(2) bond length in **1** is shorter than that in **2**. These two observations might lead to the expectation that the magnitude of k_1 for **1** should be less than that for **2**, although **1** cannot be classified as a distorted amide. The experimental result that k_1 (**2**) < k_1 (**1**) suggests that structural features alone do not sufficiently describe amide reactivity, at least for the undistorted pyrrole amides discussed here.

Wiberg and Laidig[9] described the bonding in amides to rationalise the preferred planar geometry of amides, shorter C(1)–N(2) bond lengths, that the C(1)–O(1) bond lengths were insensitive to C–N rotation, and increased electron population (calculated) at N(2) in the planar relative to the orthogonal rotamer. The interaction of n_N and π^*(C–O) results in the preferred planar geometry in the following manner. As the amide rotates from the orthogonal to the planar geometry, the hybridisation at N(2) changes from sp^3 to sp^2 to allow an improved interaction between the n_N and the π^*(C–O). This interaction must be weak, because the overall C–O bond length is scarcely affected. According to Wiberg and Laidig,[9] the sp^2 hybridised N is more electronegative than the sp^3 hybridised, resulting in a higher electron population at N in the planar rotamer. The C–N bond becomes more ionic, thus shorter and stronger.

The relative energy of the π^*(C–O) has been related to the C–N rotational barriers in amides, so it should be related to the magnitude of k_1. The HOMO of the hydroxide ion is thought to interact with the LUMO of the amide, which is the π^*(C–O). As the energy of the LUMO is increased, the energy separation between the hydroxide ion and the LUMO should also increase, resulting in a reduced k_1. For carbamates, reduced rotational barriers were attributed to the stabilising interaction between n_O and π^*(C–O). If a similar interaction between a filled p-orbital on the α–carbon and the π^*(C–O) of an amide, such as the aromatic π systems in **1** and **2**, can raise the energy of π^*(C–O) relative to some other amide, not only should the rotational barrier be reduced, but k_1 should be correspondingly decreased. In amide **1**, the toluoyl group of **2** is replaced by the *p*-nitrobenzoyl group so that the energy of the aromatic π system is lower in **1** than in **2**, and its interaction with π^*(C–O) is weaker. Thus the energy of π^*(C–O) is lower in **1** than in **2**, the π^*(C–O) can better interact with the HOMO of the hydroxide ion, and k_1 for **1** is greater than that for **2**. The evidence for such an interaction is in the crystal structures of **1** and **2**. The increased interaction of π^*(C–O) and the aromatic π system in **2** relative to **1** should destabilise the interaction of n_N and π^*(C–O) and increase the r(C–N). The increased bond length of **2** relative to **1** reflects that reduced interaction.

Esters are associated with a greater k_1 than that for the corresponding amides. This effect could be rationalised in the following way. The ester alkyl oxygen is more electronegative than the amide N, and so the *p*-type orbital on the alkyl ester oxygen interacts less than than the corresponding orbital on the amide nitrogen with the π^*(C–O) of the amide. So, the π^*(C–O) of the ester is lower than that of the amide, and is more reactive. Amide **1** has all interactions with π^*(C–O) severely reduced, lowering the energy of the π^*(C–O) relative to that of **2** and many other amides. General-base-promoted hydrolysis of esters is more common than that for the amides. General-base-promoted hydrolysis (commonly referred to as catalysis) has only been observed for the most reactive amides such as **1** and some anilides.[26] Thus, it seems that the energy of the LUMO in the amide is generally too high to allow for nucleophilic attack by water, with general-base assistance. As the LUMO energy level is lowered by the removal of the interactions with π^*(C–O) as in **1**, general-base assistance of water attack of the LUMO becomes possible. Because the LUMO of the ester is already low enough to allow the attack of water with general-base assistance, general-base promotion is observed more frequently in esters. In the serine protease, the interactions between the ser-195 and gly-193 N–H groups, and the carbonyl oxygen should lower the energy of the π^*(C–O) on the peptide. It has also been suggested that enzymes can twist the amide about the C–N bond,[25] removing the $n_N \rightarrow \pi^*$(C–O) interaction, thereby lowering the energy of the π^*(C–O).

Chapter 6

Conclusions

The occurrence of buffer catalysis was studied for the aqueous base-promoted hydrolysis of 1 in the presence of a buffer. The observed pseudo first order hydrolysis and *carbonyl*-^{18}O exchange rate constants for the hydrolysis of 1 were observed as the buffer concentration increased. These results are consistent with the general-base-promoted hydrolysis of 1. The observation of the hydrolysis to *carbonyl*-^{18}O exchange rate constants, without any added buffer, during the hydrolysis of 1 shows that To$^-$ formation is rate limiting, and this step must be catalysed by the buffer. Only one reasonable transition state can be proposed for buffer catalysis of To$^-$ formation, which is that for general-base promotion of To$^-$ formation. The ratio of the hydrolysis to *carbonyl*-^{18}O exchange rate constants with added buffer shows that buffer catalyses To$^-$ breakdown. The calculated pseudo first order hydrolysis rate constants for the hydrolysis of 1 in the absence of a buffer in the pH range 9.0–10.5, and the observed pseudo first order hydrolysis rate constants in the pH range 12–14 are consistent with hydroxide ion-promoted To$^-$ formation in both pH ranges, and hydroxide ion-catalysed To$^-$ breakdown in the upper pH range (12–14).

Results from the crystal structure of 1 suggest that structural features alone do not correlate with reactivity, at least for the planar pyrrole amides in this study. Therefore, we propose that if a replacement for the resonance model is necessary, the interaction of orbitals with the π^*(C–O) of the amide should be considered as a tool to explain the relative reactivities of the amides and carboxylic acid derivatives.

References

1. Strand, L. S. *Physiology*; Macmillan: New York, 1983; pp 29–48.

2. Vollhardt, K. P. C. *Organic Chemistry*; W. H. Freeman: New York, 1987; pp 790–821.

3. Creighton, Thomas E. *Proteins, Structures and Molecular Principles*; W. H. Freeman: New York, 1940; pp 1–6, 489–494.

4. Menger, F. M.; Donohue, J. A. *J. Am. Chem. Soc.* **1973**, *95*, 432–437.

5. Isaacs, N. S. *Physical Organic Chemistry*; Longman Scientific and Technical, John Wiley and Sons: New York, 1987; pp 255–279, 330–331.

6. Lowry, T. H; Richardson, K. S. *Mechanism and Theory in Organic Chemistry*. Harper and Row: New York, 1987; pp 676–677, 714–717.

7. Bender, M. L.; Ginger, R. D. *J. Am. Chem. Soc.* **1955**, *77*, 348–351.

8. Brown, R. S.; Bennet, A. J.; Ślebocka-Tilk, H. *Acc. Chem. Res.* **1992**, *25*, 481–488.

9. Wiberg, K. B.; Laidig, K. E. *J. Am. Chem. Soc.* **1987**, *109*, 5935–5943.

10. Deslongchamps, P. *Stereoelectronic Effects in Organic Chemistry*; Pergamon: New York, 1983; pp 101–105.

11. Bennet, A. J.; Somayaji, V.; Brown, R. S.; Santarsiero, B. D. *J. Am. Chem. Soc.* **1991**, *113*, 7563–7571.

12. Chakrabarti, P.; Dunitz, J. D. *Helv. Chim. Acta.* **1982**, *65*, 1555–.

13. Robin, M. B.; Bovey, F. A.; Basch, H. in *The Chemistry of Amides*; Zibicky, J., Ed.; Wiley-Interscience: London, 1970; pp 1–72.

14. Silverstein, R. M.; Bassler, C. G. *Spectrometric Identification of Organic Compounds*; John Wiley & Sons: New York, London, Sydney, 1967; pp 64–109.

15. Bender, M. L.; Ginger, R. D.; Unik, J. P. *J. Am. Chem Soc.* **1958**, *80*, 1044–1048.

16. Fersht, A. *Enzyme Structure and Mechanism*; W. H. Freeman: New York, 1977; pp 405–426.

17. Kahne, D.; Still, W. C. *J. Am. Chem. Soc.* **1988**, *110*, 7529–7534.

18. DeWolfe, R. H.; Newcomb, R. C. *J. Org. Chem.* **1971**, *36*, 3870-3878.

19. Brown, R. S.; Bennet, A. J.; Ślebocka-Tilk, H.; Jodhan, A. *J. Am. Chem. Soc.* **1992**, *114*, 3092–3098.

20. Bolton, P. D., *Aus. J. Chem.* **1966**, *19*, 1013–1021.

21. Bennet, A. J.; Ślebocka-Tilk, H.; Brown, R. S. *J. Am. Chem. Soc.* **1992**, *114*, 3088–3092.

22. Ślebocka-Tilk, H.; Bennet, A. J.; Hogg, H. J.;Brown, R. S. *J. Am. Chem. Soc.* **1992**, *113*, 1288–1292.

23. Schowen, R. L. *Isotope Effects on Enzyme-Catalyzed Reactions*; Cleland, W. W., O'Leary, M. H., and Northrop, D. B., Eds. University Park: Baltimore, 1977; pp 64–99.

24. Young, J. K.; Pazhanisamy, S.; Schowen, R. L. *J. Org. Chem.* **1984**, *49*, 4148–4152.

25. Fife, T. H. *Acc. Chem. Res.* **1993**, *26*, 325–331.

26. Eriksson, S. O.; Holst, C. *Acta Chem. Scand.* **1966**, *20*, 1892–1906.

27. Leffler, John E.; Grunwald, Ernest. *Rates and Equilibria of Organic Reactions*; Dover: New York, 1963; pp 20–22.

28. Heine, H. W.; Barchiesi, B. J.; Williams, E. A. *J. Org. Chem.* **1984**, *49*, 2560-2565.

29. Jolly, W. L. *Synthesis and Characterization of Inorganic Compounds*; Prentice-Hall: Englewood Cliffs, 1970; p 498.

30. Dunitz, J. D.; Winkler, F. K. *Acta. Crystallogr., Sect B.* **1975**, *B31*, 251–263.

31. Bennet, A. J.; Wang, Q.; Ślebocka-Tilk, H.; Somayaji, V.; Brown, R. S. *J. Am. Chem. Soc.* **1990**, *112*, 6383–6385.